This is a preprint manuscript for an article published in the Journal of Hydrology:
https://doi.org/10.1016/j.jhydrol.2019.124159

Flood Risk Assessment and Increased Resilience for Coastal Urban Watersheds under the Combined Impact of Storm Tide and Heavy Rainfall

Yawen Shen[1], Mohamed M. Morsy[2,3], Chris Huxley[4], Navid Tahvildari[5], Jonathan L. Goodall[6,*]

[1]Graduate Research Assistant, Dept. of Engineering Systems and Environment, Univ. of Virginia, Olsson Hall, Charlottesville, VA 22904-4742, USA. E-mail: ys5dv@virginia.edu

[2]Research Associate, Dept. of Civil and Environmental Engineering, Univ. of Virginia, Olsson Hall, Charlottesville, VA 22904-4742, USA. E-mail: mmm4dh@virginia.edu

[3]Assistant Professor, Irrigation and Hydraulics Department, Faculty of Engineering, Cairo University, P.O. Box 12211, Giza 12613, Egypt

[4]Senior Engineer, BTM WBM Pty Ltd, Level 8, 200 Creek Street, Brisbane, 4000, Australia. E-mail: chris.huxley@tuflow.com

[5]Assistant Professor, Dept. of Civil and Environmental Engineering, Old Dominion University, Norfolk, VA 23529. E-mail: ntahvild@odu.edu

[6]Associate Professor, Dept. of Engineering Systems and Environment, Univ. of Virginia, Olsson Hall, Charlottesville, VA 22904-4742, USA. E-mail: goodall@virginia.edu

[*] corresponding author: E-mail: goodall@virginia.edu, phone: +1 (434) 243-5019

Abstract

Low-lying coastal cities are vulnerable to flooding under the combined impact of storm tide and heavy rainfall. While storm tide or heavy rainfall alone is able to directly cause widespread flooding in coastal areas, often heavy rainfall and storm tide happen concurrently, and the severity of flooding is greatly exacerbated. Current methods for understanding flood risk and mapping floodplains normally does not clearly communicate either the individual or combined impact of these two flooding mechanisms. Flood mitigation strategies typically target either rainfall-driven flooding (e.g., stormwater controls) or tidally-driven flooding (e.g., flood walls and tide gates). Thus, better understanding and communicating the individual and combined flood risk resulting from these two mechanisms can be important to improving flood resilience. To address this need, this study presents tools and methods for floodplain mapping in coastal urban environments were rainfall and storm tide driven flooding can be better understood and communicated. The approaches are demonstrated for a watershed in Norfolk, VA, USA as a case study system using a 1D pipe/2D overland flow hydrodynamic model built for the watershed. Storm tide and heavy rainfall events with return periods varying from 1 to 100-year were designed based on historical observations and combined into a series of compound storm scenarios. Then these compound storm scenarios were simulated using the hydrodynamic model for simulating flow through both the land surface and underground pipe network systems. Results show how the capacity of the drainage system, and therefore flood risk reduction, is sensitive to storm tide levels, even for less extreme events with a 1-year return period. The model also provides new insights into the role of stormwater infrastructure in exacerbating flooding risk within communities during high sea level conditions. Results demonstrate how dividing the floodplain into different regions based on the dominate flooding mechanism (rainfall vs. storm tide) makes it possible to better target mitigation strategies to improve flood resilience. To this end, a transition zone index (TZI) is presented to help decision makers identify the change from rainfall-driven to tide-driven flooding for locations within a watershed. Finally, we demonstrate how different flood mitigation strategies can be tested using this modeling approach to better understand their impact on

increasing flood resilience within the system for portions of the floodplain impacted by rainfall-driven and tidal-driven flooding.

Author keywords: Coastal City; Urban Hydrology; Coastal Flood Mapping; Storm Tide; Heavy Rainfall; 2D Hydrodynamic Modeling; Flood Resilience

1. Introduction

In the context of sea level rise and climate change, flooding is one of the most challenging issues facing coastal cities today (Hallegatte et. al., 2013; Woodruff et al., 2013). Coastal cities form a vital component of national and global economies; however, coastal cities and their economies are increasingly vulnerable to extreme storm events (Hanson et al., 2011). As a consequence of extreme storm events, flooding impacts on these low-lying, densely populated, and highly developed regions can be devastating (Gallien et al., 2014; Wahl et. al., 2015; Karamouz et al., 2017; Sadler et al., 2017; Bilskie and Hagen, 2018). In coastal cities, flooding is primary caused by two processes: surface runoff due to inland heavy rainfall and tidal flooding from extreme high tide (Dawson et al., 2008; Archetti et al., 2011; Xu et al. 2014; Wahl et. al., 2015). Heavy rainfall is more likely to cause severe flooding in urban areas with poorly functioning or insufficient stormwater infrastructure (Upadhyaya et. al., 2014; Yazdanfar and Sharma, 2015). In coastal cities, rainfall-driven stormwater collected by drainage system is designed to drain into the sea either by gravity-fed flow or pumping. However, during extreme high tide events, the drainage capabilities are greatly reduced with a worse situation of backward flow. Additionally, extreme high tide alone is able to directly cause widespread coastal flooding (Xu et. al., 2014; Castrucci and Tahvildari, 2018). Thus, if heavy precipitation and extreme high tide happen concurrently, the severity of flood can be greatly exacerbated (Zheng et al., 2013; Xu et al., 2014; Wahl et. al., 2015; Karamouz et al., 2015, 2017; Wu et al., 2018). The extreme high tide discussed in this study is in the form of storm tide, which is the total observed seawater level during a storm resulting from the combination of storm surge and the astronomical tide.

Prior studies have used statistical methods to explore the interdependence between storm tide and heavy rainfall and their combined impact on flood risk (Zheng et. al., 2013; Xu et al., 2014; Wahl et. al., 2015; Batten et al., 2017; Wu et al., 2018). Zheng et al. (2013) investigated the presence of the dependence between extreme rainfall and storm surge on Australian coastline using available rainfall and tide level observations. They found a statistically significant dependence with regional and seasonal variations for the majority of studied locations. Wahl et al. (2015) studied the likelihood of concurrent storm tide and heavy rainfall for major coastal cities in the contiguous United States. It was found that the probability of combined storms is higher for the Atlantic/Gulf coast relative to the Pacific coast. Meanwhile, in many of the focused cities, the number of compound events has increased greatly over the past century, and this trend may continue under the changing environment. Xu (2014) and Batten (2017) estimated the joint probability of storm tide and extreme rainfall in their study areas and proposed design guidance for future flooding preparedness. Specifically, Batten (2017), who worked on the same region, coastal of Virginia, USA, as the current study, showed that over 50% of the rainfall events happened when sea water level was higher than mean daily high tide. While statistical approaches are important for understanding risk, they are not able to identify specific areas within a coastal community vulnerable to flooding, nor are they able to quantify how modifications to the built environment, in the form of infrastructure improvements, can mitigate flooding risk. Physical models of the system are needed for these challenges.

Coupled one-dimension (1D) pipe and two-dimension (2D) overland flood models are an efficient way to simulate urban flooding and have been widely used for assessing urban flood risk (Leandro et al., 2009; Seyoum et al., 2012; Russo et al., 2015; Fan et al., 2017; Xu et al., 2017; Martins et al., 2018). In prior studies, 1D models (Ray et. al., 2011; Lian et. al., 2013; Bacopoulos et al., 2017; Karamouz et al., 2017) or 2D models (Karamouz et al., 2017; Silva-Araya et. al., 2017) have been used to investigate the combined impact of storm tide and extreme rainfall, but the combination of 2D/1D modeling approaches to simulate both overland flow and flow through stormwater drainage systems for coastal watersheds is

93 novel. Coastal regions are usually located in low-relief terrains with flat or mild slopes and a large amount
94 of storage potential, especially in coastal cities with complex topography and a large number of artificial
95 structures. Routing water in such regions is not as straightforward as in high-gradient regions since water
96 does not always stay within river channels. In confined channels, 1D models are able to generate good
97 estimation of flooding as long as the water remains in the channels (Marks et al., 2004; Leandro et al.,
98 2009). However, for extreme storm events in urban environment, stormwater flow can easily overtops the
99 curbs in the streets, and the direction of the flow may change dramatically. In such conditions, a 2D
100 model is a more reliable tool for urban flood simulation. However, even though 2D models were used in
101 Karamouz (2017) and Silva-Araya (2017), the underground drainage system was not considered in both
102 studies. Underground drainage system is a key component of stormwater management infrastructure in
103 coastal cities, and its efficiency could be greatly influenced by the downstream tidal boundary conditions
104 (Archetti at. al., 2011). Therefore, in order to simulate coastal city flooding in a realistic manner, flood
105 models need to be capable of simulating the dynamics of flow on ground surface and pipe flow in
106 underground drainage system, as well as the interaction between them. An effective way is to use a 1D
107 pipe and 2D overland coupled model. Several commercial or open-source 1D/2D modeling system are
108 available, such as, the Two-dimensional Unsteady Flow (TUFLOW) model (Syme, 2001), MIKE 21
109 (Carr and Smith, 2006), XP-SWMM, Leandro (2016), and Wu (2017). Such modeling systems can
110 support coastal flood mapping with the consideration of the individual and combined flood risk resulting
111 from storm tide and heavy rainfall, and it can be important to improving flood resilience by testing the
112 impact of different potential mitigation strategies.

113 In prior studies, geospatial information and hydrodynamic models have been used for
114 understanding flood risk and mapping coastal floodplains (Wang et al., 2002; Karamouz et al., 2015;
115 Karamouz et al., 2017; FEMA, 2018). However, these methods normally do not clearly communicate the
116 mechanisms of flooding for specific locations. In other words, it is not clear if the flooding is caused by
117 the individual or combined impact of storm tide and heavy rainfall. This is problem in part because flood

mitigation strategies typically target either rainfall-driven flooding (e.g., stormwater controls) or tidally-driven flooding (e.g., flood walls and tide gates). To access flood risk across coastal landscapes, Bilskie and Hagen (2018) proposed a methodology to delineate coastal floodplains into three flood zones, tidal zone, hydrological zone, and transition zone, according to different driving forces of flooding. The transition zone is defined as an area susceptible the interaction between tidal and rainfall-driven flooding. Application of this method to a flooding event in southeast Louisiana shows that the excess rainfall and storm surge interact nonlinearly and their compound effect is smaller than their superposition (Bilskie and Hagen, 2018). Their study area was primarily located in a rural area with no effect from underground stormwater drainage systems. The transition zone identified from their study is primarily located in a region relatively close to the shoreline, where the tide has a significant impact on flooding. However, in urban environments, the interaction between rainfall-driven flooding and tidal flooding exists on both the land surface and subsurface through stormwater pipeline drainage systems. Thus, the influence of storm tide is not limited to the near-shoreline region, but regions further inland as well.

The objective of the study is to develop methodologies to enhance the understanding of the coastal city flood risk and how flood mitigation strategies in improving flood resilience. A high-resolution, coupled 1D pipe/2D overland hydrodynamic model was built using the TUFLOW modeling system for a watershed within the Hague community of Norfolk, VA, USA. TUFLOW solves the full 2D depth averaged momentum and continuity equations for shallow water free surface flow, and incorporates the full functionality of the ESTRY one-dimensional (1D) hydrodynamic network (Syme 2001). This modeling system outputs detailed flooding information on both land surface and underground pipeline system, which allows one to assess flood risk and understand the contribution of flooding from individual or combined factors. The coastal floodplain mapping method proposed in Bilskie and Hagen (2018) was extended for a coastal urban watershed based 2D/1D flood model simulations. The spatial extent of the transition zone was identified using different combinations of storm tide and heavy rainfall events. We also introduce an index to represent the likelihood of a region being susceptible to the combined impact of

storm tide and heavy rainfall. The mapping strategy assists in understanding how flood mitigation approcah reduces flooding risk resulting from rainfall and storm tide drivers. The 1D pipe/2D overland flood model is also a powerful tool to evaluate the efficiency of different flood mitigation strategies. As a demonstration, two flood mitigation methods are tested in this study. The methodologies developed in this study can aid city planners and stormwater engineers in other coastal communities to understand and improve flood resilience by targeting both rainfall and storm tide-driven flooding.

The remainder of the paper is organized as follows. The methodology section provides background information about the study domain and explains the urban flood model and design the storm scenarios used in the study. It also includes a description of how flood zones were determined within the floodplain mapping analysis and introduces the concept of a transition zone index (TZI). The results and discussion section explains the model evaluation, how the lag between the peak storm tide and rainfall was determined in the modeling scenarios, and flood risk determined by the model. The influence of storm tide on the underground stormwater drainage system is also explored, followed by the coastal floodplain mapping results and a brief exploration of how flood mitigation strategies could reduce the floodplain for the study watershed. The paper concludes with key findings along with possible future research to further advance the approach.

2. Methodology

2.1 Study area

Norfolk, Virginia, USA is the second most populous city in Virginia and the home of world's largest naval base. Norfolk is a highly urbanized and relatively flat community with nearly all areas below elevation 4.5m (North American Vertical Datum of 1988: NADV 88). The relative low elevations and tidal connections to the Chesapeake Bay place a significant percentage of the city at risk of tidal flooding. The tidal flooding risk is more serious under the threat of sea level rise (SLR) and land subsidence (Li et. al., 2013; Sadler et. al., 2017). The study domain is located in the Hague community of the Norfolk, VA

(Figure 1). The sources of spatial datasets used in this study are provided in Table 1. The study domain has a total area of 3.7 km^2, including total waterbody area of 0.1 km^2 and land area of 3.6 km^2, in which 0.7 km^2 is building area. Ground surface elevation of the study domain varies from 0.3m to 4.2m with an average of 2.6m (NAVD88).

Table 1. Spatial Datasets Collected to Build the Urban Flood model

Spatial Dataset	Provider	Sources
LIDAR DEM	VGIN	https://www.vita.virginia.gov/integrated-services/vgin-geospatial-services/elevation---lidar/
Land Cover	VGIN	https://www.vita.virginia.gov/integrated-services/vgin-geospatial-services/land-cover/
Basin Boundaries	Norfolk City	https://www.norfolk.gov/index.aspx?NID=1605
Drainage System	Norfolk City	https://www.norfolk.gov/index.aspx?NID=1605
Building Outlines	VGIN	https://www.arcgis.com/home/item.html?id=994d0afa44c046498f9774613671ce9a
Road Centerlines	VGIN	https://www.vita.virginia.gov/integrated-services/vgin-geospatial-services/transportation/

Note: VGIN: Virginia Geographic Information Network

In this study, the tide level data was collected from the Sewells Point station (Station ID: 8638610), which is 9.7km away from the domain tidal boundary. This tide gauge has the longest tide level record, dating back to 1927, in Virginia. There is no official rain gauge located inside the study domain. Rainfall data was obtained from two weather stations run by the U.S. National Weather Services (NWS) and two other weather stations run by the Hampton Roads Sanitation District (HRSD) (Figure 1). On average, the NWS and HRSD stations are about 9km and 3km away from the study domain center, respectively. The two NWS weather stations have hourly rainfall data available since 1948 and 1973, respectively. The HRSD stations were installed in January 2016. For hurricane events simulated the study, the NWS rainfall record was used as rainfall input for hurricanes earlier than 2016, and the HRSD rainfall record was used for hurricanes after 2016.

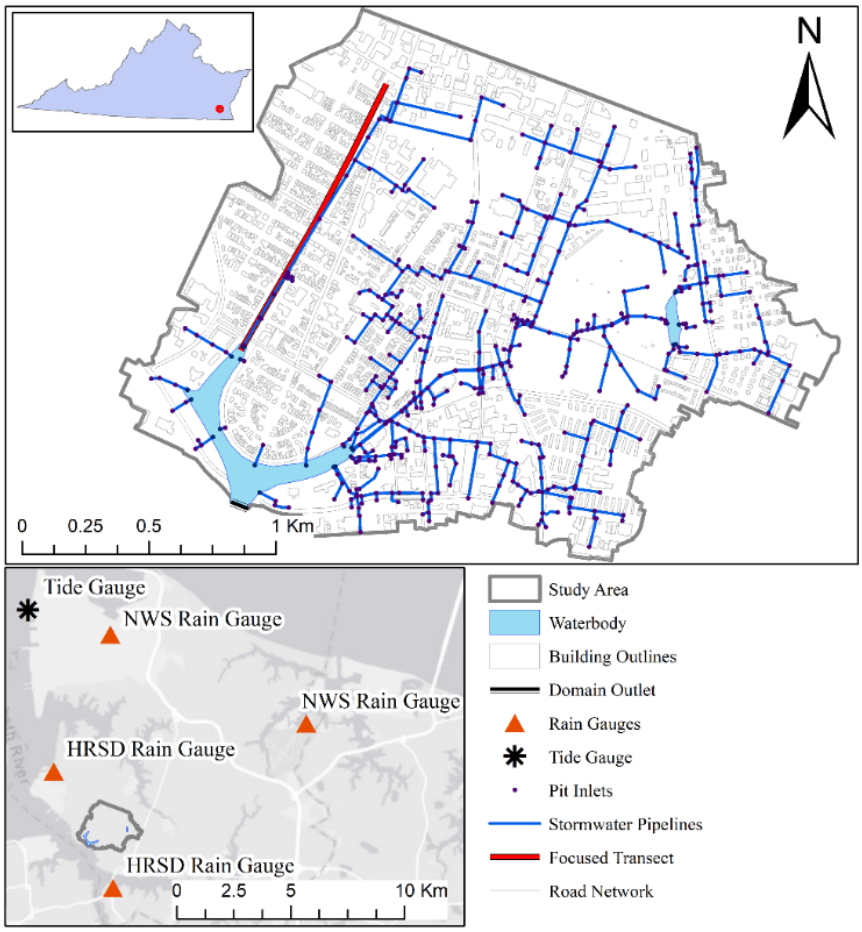

Fig. 1. Study area with tide gauge and rain gauge locations.

2.2 The Urban Flood Model

The study domain is located in a highly urbanized area with complex flow patterns and paths. The interaction between overland flow and pipe flow significantly increases the complexity of flood modeling. To overcome these difficulties, a 1D pipe/2D overland hydrodynamic flood model was built using the TUFLOW model. TUFLOW was chosen due to its capability to represent surface flow on a 2D domain as well as fluvial and pipe network via its 1D functionality and the dynamically link between the two. The TUFLOW High-performance Computing (HPC) engine allows to execute the model on multiple GPU units, which would significantly speed up model simulations.

193 The domain boundary was selected from the basin boundaries provided by the City of Norfolk,
194 and adjusted based on a high resolution LiDAR digital elevation model (DEM) and the underground
195 drainage system. There is no rainfall-driven flow, in the form of overland or pipe flow, entering into the
196 study domain from adjacent watersheds. Therefore, all rainfall-driven flooding is generated inside the
197 domain. The outlet of the domain connects to the Elizabeth River, which is a portion of the Chesapeake
198 Bay. Wave speed of tide is currently not considered in this study. So, the tide level at Swells Point was
199 considered to be the same as the outlet of the study watershed. The topography of the 2D domain was
200 defined using a $1m \times 1m$ Lidar DEM, building outlines, and road centerlines collected from the Virginia
201 Geographic Information Network (VGIN), as shown in Table 1. A land cover dataset with 1m spatial
202 resolution was obtained from VGIN to define the overland roughness. The Manning's roughness
203 coefficients for overland flow from McCuen (1998) were assigned to the 2D domain based on the land
204 cover types, as shown in Table 2. For a small watershed, flooding is primarily from short-duration
205 extreme storm events (Bryndal et al., 2017). At the same time, the current study area has an
206 imperviousness ratio of 57% and shallow groundwater level. Thus, infiltration is expected to have minor
207 influence on flooding caused by extreme storm events. Therefore, infiltration was not considered in the
208 current version of the urban flood model, which presumes saturated conditions within the watershed prior
209 to the model simulation period.

210 Table 2. Parameters used in the 1D pipe/2D overland hydrodynamic model

Parameters	Type	Value
Manning's n value of 2D overland surface	Asphalt	0.012
	Concrete	0.013
	Other urban feature	0.012
	Grassland	0.15
	Shrub land	0.4
Manning's n value of 1D pipelines	Plastic pipes	0.012
	Concrete pipe	0.014
	Cast iron pipe	0.013
	Corrugated-metal pipe	0.015
	Brick	0.014

TUFLOW solves the full 2D depth averaged momentum and continuity equations for shallow water free surface flow, and incorporates the full functionality of the ESTRY one-dimensional (1D) hydrodynamic network (Syme 2001). In TUFLOW, inlets and grates are represented as pits, which allow modelers to specify a depth-discharge relationship between ponding depth at pits and flow rate entering drainage system. The depth-discharge relationship, controlled by the type and dimension of inlet, defines the flow rate of overland stormwater entering into the pipeline system. The urban drainage design manuals from Federal Highway Administration (2009) and state departments of transportation (e.g.: VDOT, 2017) provide methods to calculate the draining capacity corresponding to the type and dimensional of different inlets. In this study, the depth-discharge curves were determined for different types of inlets based on the VDOT Drainage Manual (2017). The initial pipeline entrance and exit energy loss coefficients are set as value of 0.5 and 1.0, respectively. TUFLOW is capable of automatically adjusting energy loss coefficients associated with the contraction and expansion of flow into and out of a structure according to the approach and departure velocities in the upstream and downstream channels. Details of the energy loss adjustment technique are included in TUFLOW manual (2016) and Tullis and Robinson (2008). The Manning's roughness coefficients were assigned to different types of pipelines, as shown in Table 2.

2.3 Designing of Combined Storm Events

This study focuses on storm tide and heavy rainfall occurring with hurricanes on the Virginia coastline. A summary of the hurricane history of central and eastern Virginia is provided by the National Weather Service (NWS, 2016). Flood risk as a consequence of storm tide and heavy rainfall with the return periods varying from 1 to 100-year are simulated and investigated in this study. Thus, hurricanes, resulted in both storm tide and rainfall with recurrence intervals less than one year for coastal Virginia, were filtered out from the list of hurricanes analyzed in this section. Historical hurricanes with rainfall and tide peak recurrence intervals greater than one year are listed in Table 3. Hourly rainfall data were collected from the NWS weather station 013737 due to it having the longest record in the study region. The Sewells

Points station was installed in 1927 to collect tide level data, thus only hurricanes happened after 1927 are listed in Table 3. For the 15 hurricanes with an available rainfall record, the total amount of rainfall varies from 16.8mm to 289.9mm. The minimal and maximum tide peaks are 0.55m and 1.95m (NAVD88), respectively. The rainfall durations of the 15 hurricanes vary from 8 to 77 hours with the median of 22 hours. Ten out of the 15 hurricanes have rainfall durations between 16 to 30 hours. Therefore, because rainfall events happening during hurricanes in the Virginia coastal region have average durations of about 22 hours. A 24-hour duration was selected as the design rainfall events in this study.

Table 3. Historical hurricanes in Virginia with return period of rainfall or storm tide greater than one year.

Year	Storm Event	Rainfall Duration (hrs)	Total Rainfall (mm)	Peak Tide Level (m, NAVD88)
1928	Unnamed	--	--	1.13
1933	Unnamed	--	--	1.95
1936	Unnamed	--	--	1.56
1953	Barbara	--	--	0.83
1960	Donna	22	109.6	1.22
1964	Cleo	24	289.9	0.55
1964	Dora	30	122.0	1.19
1971	Doria	22	78.6	0.61
1985	Gloria	18	143.6	1.04
1986	Charley	16	27.5	1.13
1998	Bonnie	14	92.8	1.20
1999	Floyd	33	166.5	1.29
2003	Isabel	8	16.8	1.91
2004	Charley	15	94.6	0.80
2006	Ernesto	27	256.6	1.19
2011	Irene	27	207.7	1.81
2012	Sandy	77	151.8	1.57
2016	Hermine	20	68.2	1.38
2016	Matthew	21	234.7	1.27

2.3.1 Designing of Storm Tide Events

The annual exceedance probability curves of extreme tide levels for the Sewells Points station were generated by the U.S. National Oceanic and Atmospheric Administration (NOAA) (https://tidesandcurrents.noaa.gov/est/curves.shtml?stnid=8638610). The annual exceedance probability

curves of extreme tide levels with 95% confidence intervals are included in the report. The curves were calculated from the annual highest tide levels after the mean sea level trend was removed. The tide levels with different return periods along with the 95% confidence intervals are obtained from the NOAA report as shown in Table 4. The tide level was converted from the Mean Higher High Water (MHHW) datum to NAVD88 to be consistent with the urban flood model settings.

Table 4. Annual exceedance probabilities and return periods of extreme tide levels and the matched historical hurricanes.

Exceedance Probability		99% (1-Yr)	10% (10-Yr)	2% (50-Yr)	1% (100-Yr)
Tide Level (m, NAVD88)		0.78	1.56	1.87	2.06
95% Confidence Intervals		0.72 - 0.81	1.35 - 1.61	1.64 - 2.33	1.76 - 2.74
Historical Hurricanes	Name	Charley (2004)	Unnamed (1936)	Isabel (2003)	Unnamed (1933)
	Tide Peak Level (m)	0.8	1.56	1.91	1.95

The tide level time series observed during historical hurricanes are taken as the references for designing storm tide events. Tide peak levels were selected as an indicator to choose historical hurricanes as reference to design storm tide events. For storm tides with certain return periods in Table 4, the matched hurricane events in Table 3 have tide peak levels that are close to the storm tide peaks and fall in between the 95% confidence intervals. The tide level observations of the matched hurricanes would be taken as the designed storm tide events. Take the 50-year storm tide event as an example. According to Table 4, the 50-year tide has a peak of 1.87m (NAVD88) with 95% confidence intervals from 1.64m to 2.33m. In the Table 3, Hurricane Isabel (2003) had a tide level peak of 1.91m, which is closest to the 50-year tide among all these hurricanes. At the same time, the tide peak level of Hurricane Isabel (2003) falls in between the 95% confidence interval of the 50-year tide. Therefore, Hurricane Isabel (2003) was selected as the 50-year storm tide event in this study, and its tide level observation was used to design the 50-year storm tide event. Designed storm tide events with return periods of 1, 10, 50, and 100 years are presented in Figure 2.

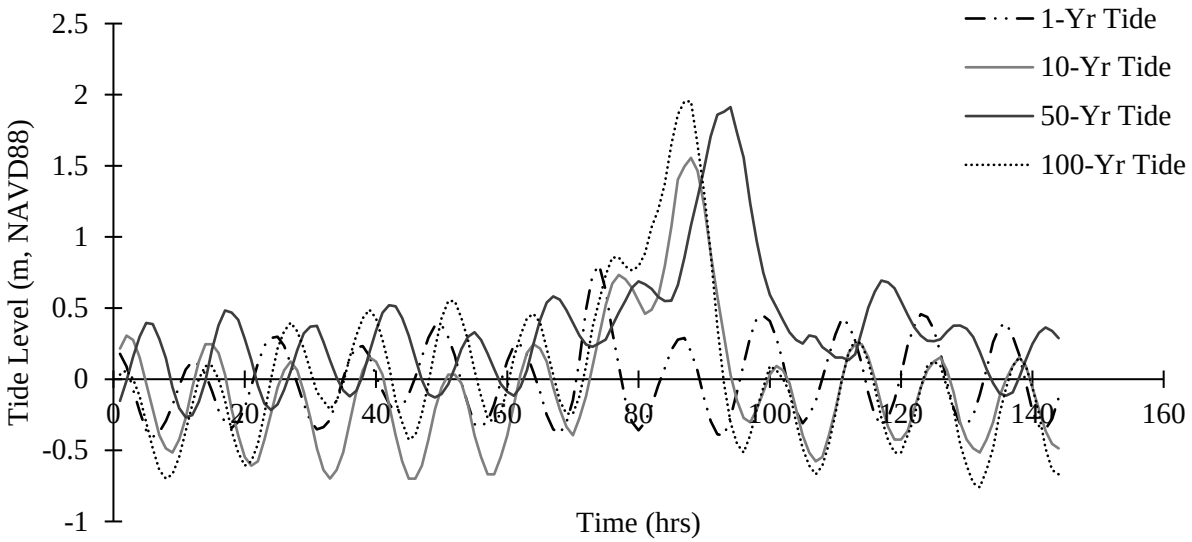

Fig. 2. Designed storm tide events with different return periods.

2.3.2 Designing of Heavy Rainfall Events

In this study, the rainfall intensity-duration-frequency (IDF) curves were obtained from the NOAA Atlas 14 precipitation frequency estimates (Bonnin et. al., 2006). The NOAA Atlas 14 contains precipitation frequency estimates with associated confidence intervals for the United States, and it is provided through a web site (https://hdsc.nws.noaa.gov/hdsc/pfds/pfds_map_cont.html). The 24-hour rainfall intensities with the 90% confidence intervals for different return periods were obtained from the NOAA Atlas 14 and are shown in Table 5.

Table 5. NOAA Atlas 14 precipitation frequency estimates with 90% confidence intervals.

Exceedance Probability	99% (1-Yr)	10% (10-Yr)	2% (50-Yr)	1% (100-Yr)
24-Hr Rainfall Intensity (mm)	74	140	202	234
90% Confidence Intervals (mm)	69 - 81	129 - 152	183 - 218	210 - 253

The rainfall distribution used for rainfall design storms was obtained from a Natural Resources Conservation Service (NRCS) study (Merkel et al., 2015). In Merkel's study (2015), four types of rainfall distributions were developed from data in the NOAA Atlas 14. A map showing a multistate area with groups of regional precipitation distributions was presented along with tables containing 24-hour precipitation distributions in Merkel's study (2015). The current study domain is located in the region of

Type C precipitation distribution. The precipitation distribution is non-dimensional between values 0 to 1.0. Designed rainfall events were generated by multiplying the Type C precipitation distributions with the corresponding 24-hour rainfall intensities from the NOAA Atlas 14. The synthetic rainfall events with different return periods are presented in Figure 3.

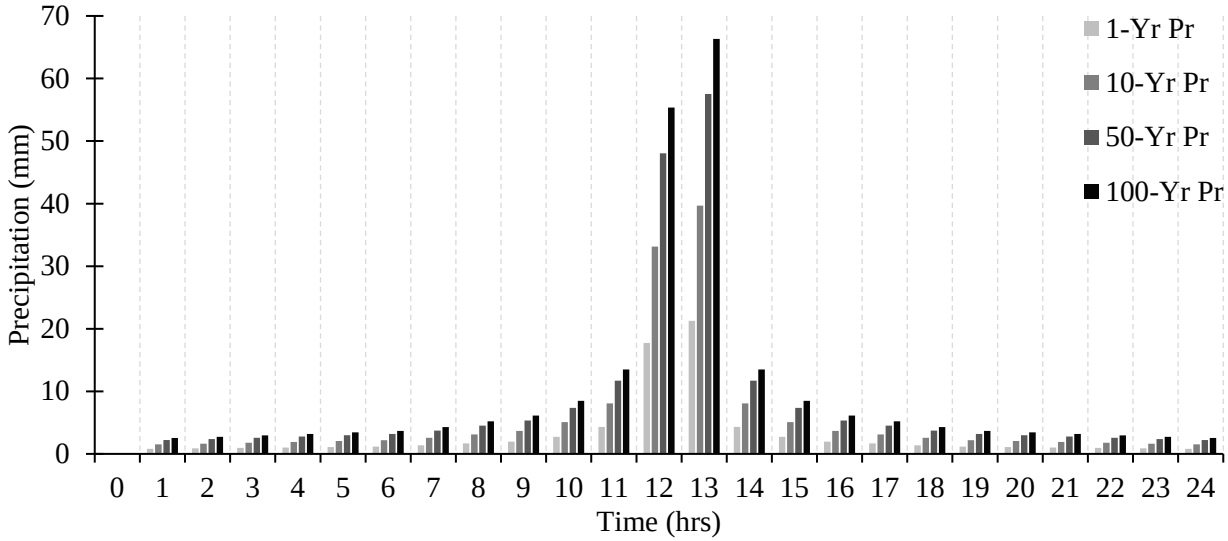

Fig. 3. Synthetic 24-hour heavy rainfall events with different return periods.

A series of compound storm scenarios were created by combining different synthetic storm tide and heavy rainfall events. The combined impact of storm tide and heavy rainfall are investigated according to the urban flood model simulation for these storm scenarios. Flood simulations on both 2D land area and 1D pipelines were generated as outputs.

2.4 Determine Food Zones

According to Bilskie and Hagen (2018), the coastal floodplain can be separated into three different flood zones, hydrological zone, tidal zone, and transition zone, based on the driving forces of flooding. In the tidal zone, storm tide is the primary factor of flooding and rainfall has negligible impacts. The tidal zone is usually located near a shoreline. The hydrological zone, normally located inland, is dominated by rainfall-driven flooding with only minor impacts from storm tide. The transition zone is where significant interactions exist between rainfall-driven and tidal flooding.

These three flood zones for a specific combined storm event are determined by the maximum water level simulations from three designed storm scenarios. In Simulation I, the storm tide is the only input, i.e., no rainfall input. Simulation II consists of heavy rainfall input with a normal tide. Normal tide means an average astronomical tide that cannot cause flooding in the study domain, and its maximum tide level is lower than all drainage pipeline outlets. Simulation III consists of both storm tide and heavy rainfall. Thus, flooding in Simulations I and II is driven by storm tide and rainfall, respectively, and it is driven by the combined effect of storm tide and rainfall in Simulation III. In the tidal zone, rainfall has negligible impacts on flooding; thus, the maximum water level simulation from Simulation III would have minor differences compared to Simulation I even with the existing of rainfall impact. Therefore, the tidal zone is defined as the area where the maximum water level simulations from Simulations I and III have a difference equal to or smaller than 0.01m. In the hydrological zone, storm tide has minor impacts on flooding. Therefore, the maximum water level simulations from Simulation II and III would be fairly close in the hydrological zone. In the current study, the hydrological zone is identified as the area where the maximum water level simulations from Simulation II and III have a difference equal to or smaller than 0.01m. The transition zone is normally located in between the hydrological and tidal zones. In the transition zone, both the maximum water level simulations from Simulation I and II are smaller than Simulation III with a difference greater than 0.01m.

The spatial extent of the transition zone varies with the change of storm tide and heavy rainfall combinations. Thus, simply mapping this zone does not fully describe this complex interaction between storm tide and heavy rainfall. In general, a greater tide peak or rainfall intensity would lead to a larger transition zone. For compound storms with higher tide peaks, the tidal zone and transition zone is more likely to extend further inland. Meanwhile, the increase of rainfall intensity would shrink the spatial extent of the tidal zone. To quantify this interaction, we defined the transition zone index (TZI) as

$$TZI = \frac{M}{N} \quad (1)$$

where, M is the number of simulations with transition zones sharing a same location, and N is the total number of simulations. TZI can be computed for any watershed based on the simulations from all the compound storm scenarios, as demonstrated in this study. A high TZI locates an area in the watershed where flooding is the product of interactions between storm tide and heavy rainfall. The higher the TZI, the stronger the interaction between these two primarily mechanisms for coastal flooding. TZI helps to identify regions in the watershed that would be impacted by flood mitigation approaches that target either storm tide driven flooding or rainfall driven flooding.

3. Results and Discussion

3.1 Model Evaluation

Observations of the depth, extent, and duration of flooding in urban coastal landscapes are very rare; however, such data are essential to evaluate the performance of urban flood models (Smith et al., 2012). Data sources, such as photographs taken of flooded areas, newspaper reports and personal interviews, flood information collected from social media, and crow-sourced drone footage, can be converted to inundation information for model evaluation (Smith et al., 2012; Middleton et al., 2014; Fohringer et al., 2015; Loftis et al., 2017). However, these data sources are often sparse and not available for the current study domain. In the current study, the data source used for flood model evaluation is a crowdsourced flood report dataset from the City of Norfolk, VA. This record includes flooded street locations in Norfolk starting from Hurricane Nicole on 30 September 2010 (Salder et al., 2018).

In the flood report record, only the date and location of reports were stored instead of the precise time and flood depth. Therefore, the maximum inundation maps on the date when flood locations were reported were compared with the flood report locations as an indication of model performance. During a storm event, stormwater may cause ponding on the most parts of the study domain. Ponding depth is selected as the indicator for inundation area mapping in this study. The inundation maps shown in this paper only include area with ponding depth greater than 0.1 m. This value was selected to distinguish

between dry land and flooded locations during storm events. It is assumed that the impact of flood is negligible for flood management purpose when the water depth is smaller than 0.1m.

The model performance was evaluated on Hurricanes Irene (2011), Hermine (2016), and Matthew (2016) (Figure 4). If simulated ponding exists in a 20m buffer of a flood reported location, this flood report was assumed to validate the model simulation. All flood reported locations of Hurricanes Irene and Matthew are consistent with the inundated areas from the simulations. During Hurricane Hermine, 25 flood locations were reported, and 22 (88%) locations matched with the flood model simulation. The remaining three flood locations are about 250 m away from the shoreline as shown in Figure 4(b). The ponding depth at these three locations varies from 0.05 m to 0.09 m, which is lower than the cutoff depth selected for inundation area mapping. The crowdsourced flood report dataset contains unique and valuable street-level flood information, but there are still limitations of this dataset. As can be expected when using crowd-sourced data, the flood report dataset has an unknown amount of subjectivity and bias because the flood locations are reported by individuals (Sadler et al., 2018). Nonetheless, using the best available information, it is reasonable to suggest that the urban flood model has predictive skill at simulating flooded roads for three different extreme weather events.

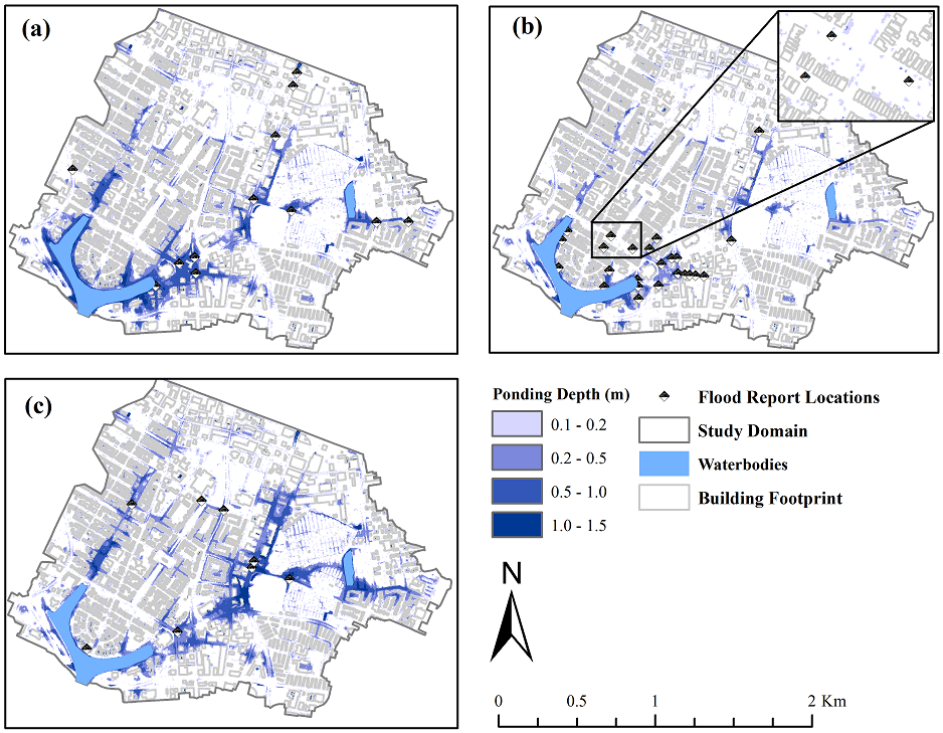

Fig. 4. Ponding depth on time of maximum inundation area and flood report locations for hurricanes (a) Irene (2011), (b) Hermine (2016), and (c) Matthew (2016)

3.2 Time Lag between Storm Tide and Rainfall

The storm scenarios were created by combining the synthetic rainfall and storm tide events; however, we needed a method to match the time axis of rainfall and storm tide events. Usually, there is a time lag between storm tide and rainfall events, and the time lag has a significant impact on flood risk (Zheng et al., 2013). In this section, we show how the time lag between the tide peak and rainfall peak influence flood risk in the study domain.

Time lag is defined as

$$T_{Lag} = T_{Tide\ Peak} - T_{Rainfall\ Peak} \quad (2)$$

where $T_{Tide\ Peak}$ is the time of tide peak and the $T_{Rainfall\ Peak}$ is the time of rainfall peak. In this analysis, the 10-year rainfall is selected as an intermediate rainfall intensity. The 1 and 10-year storm tides were chosen to represent a short duration (less than 6 hours) and a long duration (greater than 6 hours) storm tide, respectively. For each combination of storm tide and heavy rainfall, 17 synthetic storm

scenarios with time lags varying from -8 to 8 hours were created and simulated. The maximum inundation areas (MIA) in percentage of the total land area and the maximum flood volumes (MFV) on land are shown in Figure 5. The tide levels at the time of rainfall peak for each scenario are provided on the upper row of Figure 5. For both the 1-year tide and 10-year tide cases, the MIAs appear when tide peaks and rainfall peaks happen simultaneously, i.e., time lags equal to zero. The MFVs occur when rainfall peaks are one hour ahead of tide peaks (time lags equal to one). From Figure 5, we found that both MIA and MFV have positive correlations with tide levels at the time of rainfall peaks. When the absolute values of time lag are greater than 4 hours, rainfall peaks happen at low tide periods, and both MIA and MFV are relatively small. For scenarios with absolute values of time lag less than 4 hours, the MIA and MFV increase rapidly with the increase of tide levels at rainfall peaks. Using MIA and MFV as indicators, it the worst flooding appears to happens when the time lags are between -1 to 2 hours. In the current study, the compound storms with simultaneous storm tide and rainfall are chosen to represent the worst-case scenarios, where the worst-case scenarios are determined by using the MIA as the indicator of flood severity.

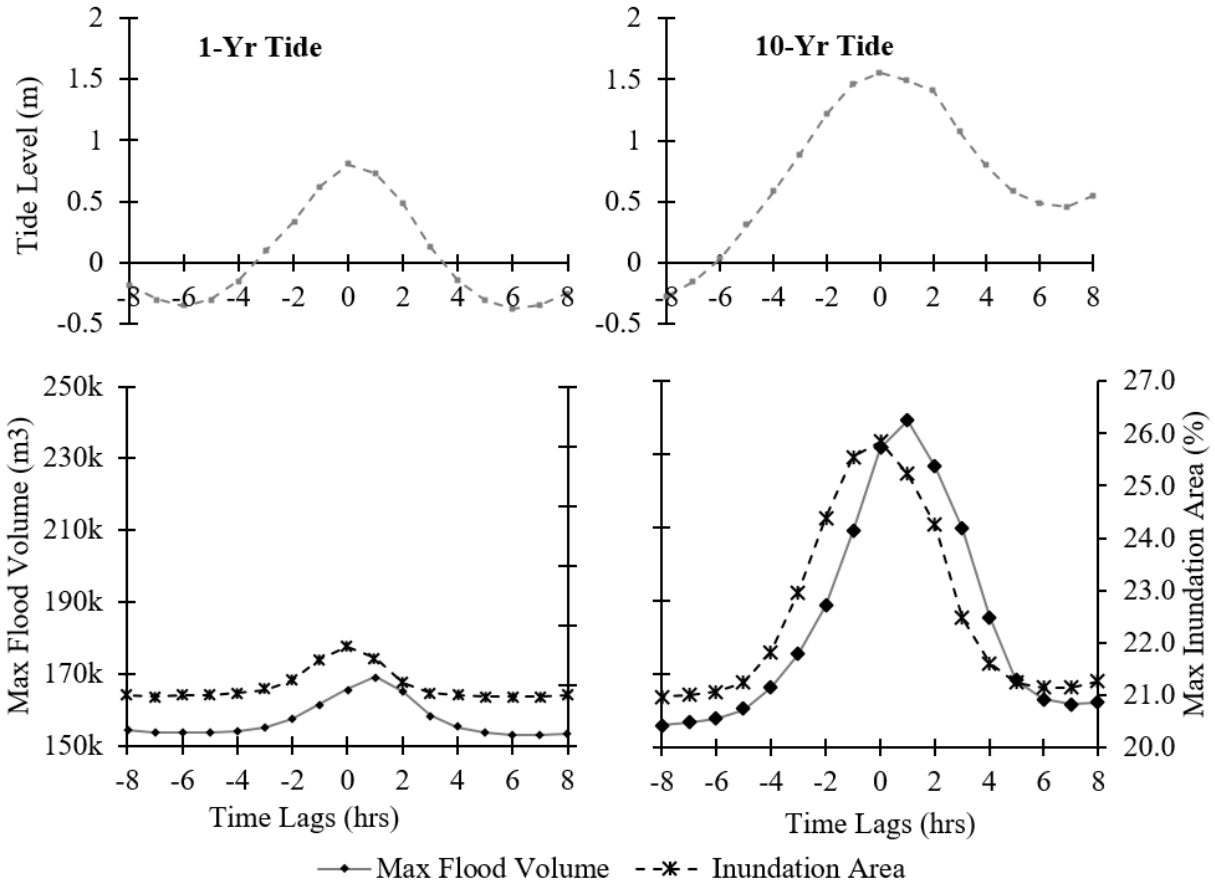

Fig. 5. Influence of time lag between storm tide and rainfall on flood risk with the examples of 10-year rainfall event pairing with 1-year and 10-year storm tide events.

3.3 Flood Risk

The flood ponding depth at the time of maximum inundation area for each storm scenario is presented in Figure 6. Among all storm scenarios, the maximum ponding depth of 1.49 m appeared during the compound storm of 100-year rainfall and 100-year tide. For storm scenarios with fixed rainfall intensity, for example, 1-year rainfall, the inundation area and ponding depth near the shoreline increase rapidly as the storm tide return period increases. Several inland flood-prone areas are isolated from overland tidal flooding; however, for a specific rainfall intensity, both the inundation area and ponding depth in these areas experience a significant increase as the storm tide return period increases. Flooding in these flood-prone areas are greatly influenced by the impact of storm tide on underground pipeline system, which will be discussed in detail in the Section 3.5.

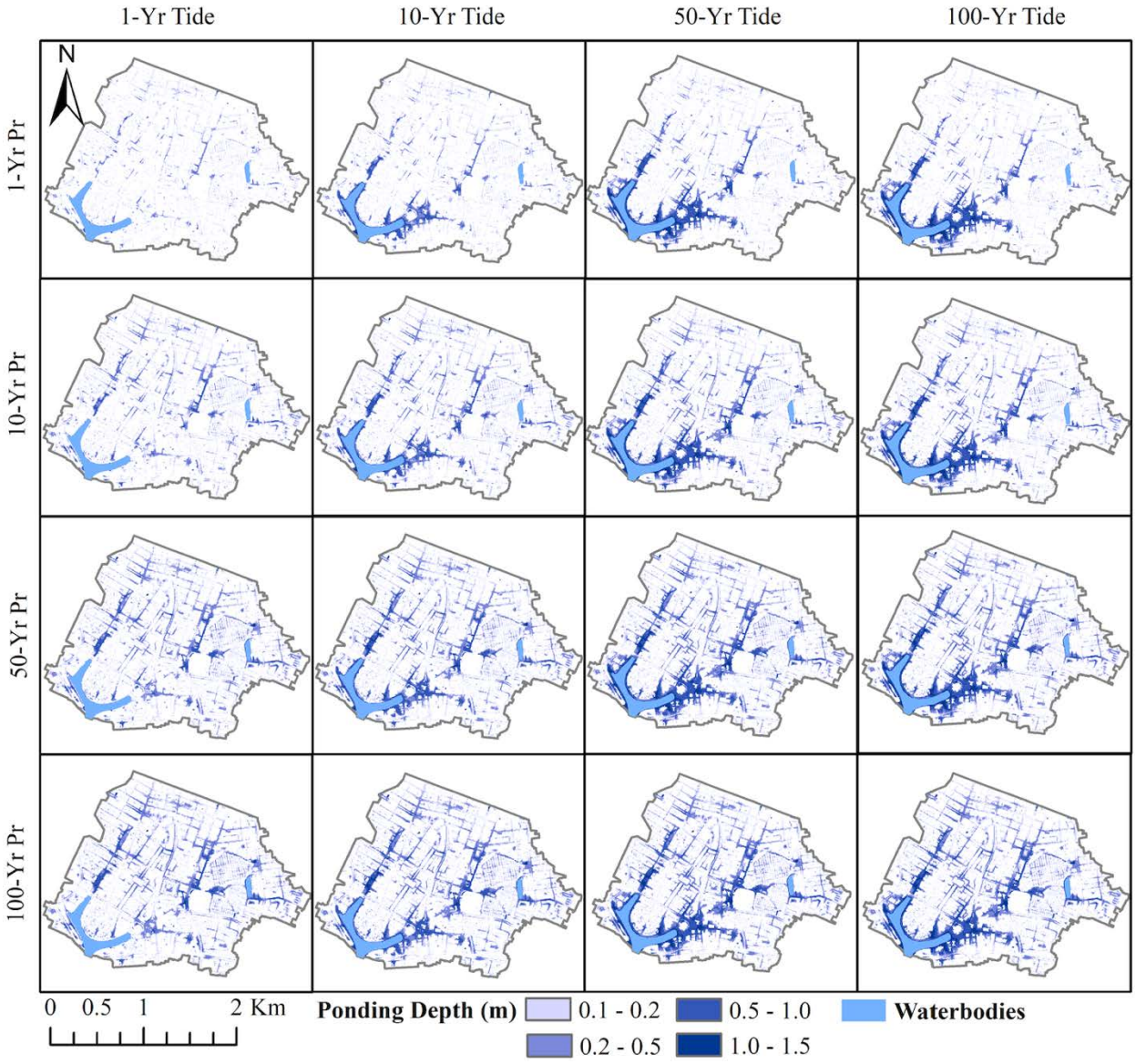

Fig. 6. Combined impact of storm tide and heavy rainfall on flood ponding depth at the time of maximum inundation area.

MIAs and MFVs for different compound storm scenarios are provided in Figure 7. The storm scenario with the 1-year rainfall and 1-year storm tide would flood 12.7% of the land area with a MFV of about $76{,}000m^3$. The storm scenario with the 100-year rainfall and 100-year storm tide, according to the model, would cause MIA of 38.9% and MFV of about $457{,}000m^3$. From Figure 7, the results show that MIA is more sensitive to the change of rainfall return period compared to tide return period. For example, under the 1-year storm tide condition, MIA increases from 12.7% for 1-year rainfall to 32.1% for 100-year rainfall. In contrast, for the 1-year rainfall event, MIA increases from 12.6% to 22.7% for 1 and 100-

year storm tides, respectively. From Figure 7, MFV is susceptible to the change of both rainfall intensity and storm tide severity. The simulations from certain storm scenarios have a similar amount of MIAs or MFVs but different spatial extents. For example, the difference between MIAs for the storm scenario with the 10-year rainfall and 1-year tide and the storm scenario with the 1-year rainfall and 50-year tide is only 0.7%. However, Figure 7 shows that these two scenarios, while having a similar MIA, have large differences in the spatial extent of inundated areas. As expected, the flooded area of the event with a 1-year rainfall and 50-year tide is primarily concentrated near the shoreline while the event with 10-year rainfall and 1-year tide has flooded areas more inland with relatively shallow ponding depths.

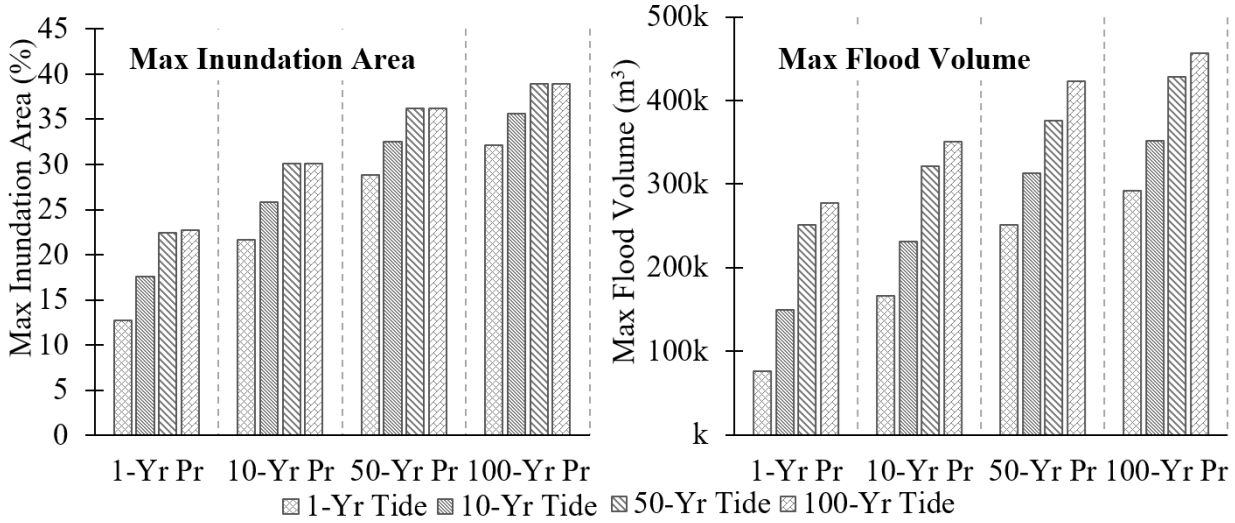

Fig. 7. Maximum inundation area in percentage of land area and maximum flood volume on land for different storm scenarios.

3.4 Influence of Storm Tide on Underground Drainage System

The study domain has a complex drainage system, which plays a key role in the stormwater management. Model results and local knowledge of the drainage system both suggest that the efficiency of the drainage system is highly sensitive to the tide levels at the outfalls. During storm tide events, the pipeline outfalls can be partly or even fully submerged. In a submerged state, both the head difference between upstream and downstream pipes and the capacity of the system are reduced, which slows the draining of stormwater through the system.

In the study domain, the ground elevation of several roads and streets near the shoreline is higher than surrounding areas. These connected roads and streets form a barrier impeding overland tidal flooding entering into inland regions. The area in between the shoreline and these elevated roads and streets is defined as the shoreline floodplain. Inside the shoreline floodplain, inundation is the combined consequence of overland tidal flooding, local rainfall-driven flooding, and surcharge flow from the underground pipeline system. The inland region is free from overland tidal flooding. Thus, the inundation in the inland region is a consequence of local rainfall-driven flooding and surcharge flow from underground pipelines. Therefore, in the inland region, the flood severity for a fixed rainfall event is determined by the efficiency of the underground pipeline system, which is highly sensitive to the tide levels at outfalls. To explore the relationship between tide level and the efficiency of the drainage system, the flood severity in the inland region is analyzed under the impact of different storm tide events. In this section, the compound storm scenarios with 1-year rainfall and storm tide varying from normal tide to 100-year tide were simulated and analyzed. Normal tide means an average astronomical tide that cannot cause flooding in the study domain, and its maximum tide level is lower than all drainage pipeline outlets. As shown in Figure 8, the maximum extent of the shoreline floodplain for these compound storm scenarios are covered by the shoreline floodplain mask, and the inland region is outside the mask. The focus pipes connect the inland region with the shoreline floodplain.

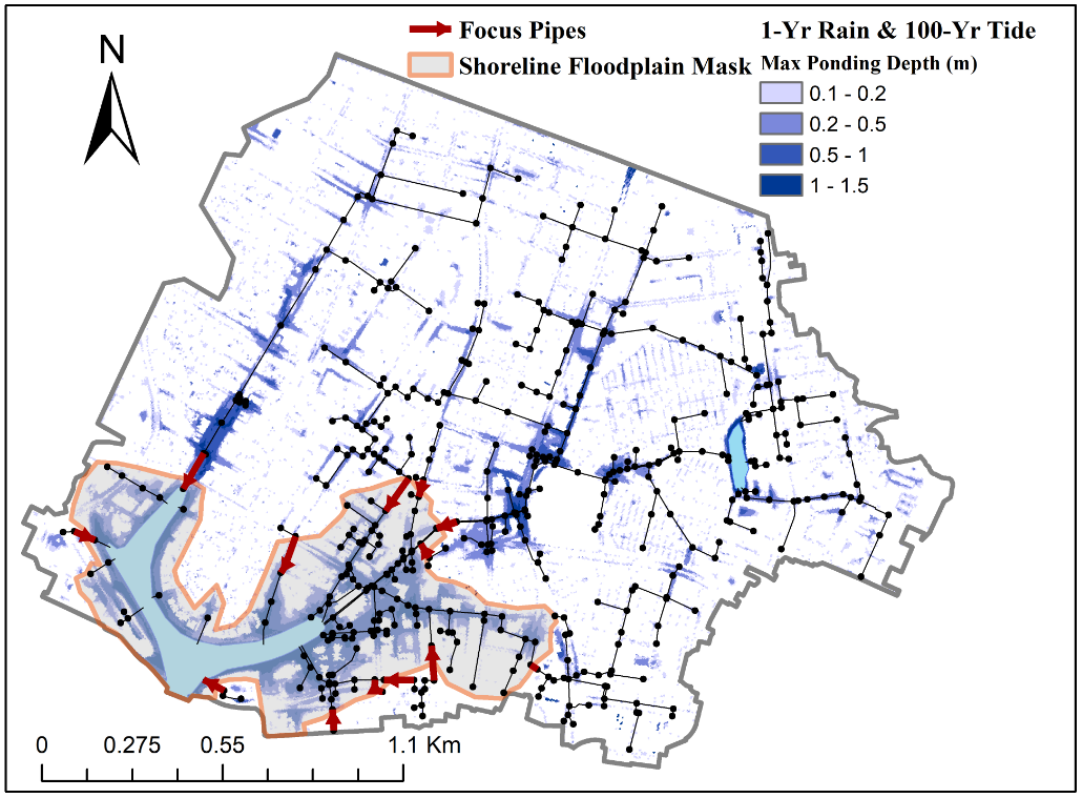

Figure 8. Locations of shoreline floodplain and focus pipes

The time series of total discharge in the focus pipes and the total amount of flood volume in the inland region for the simulated compound storm scenarios are present in Figure 9. From Figure 9 (a), there is no backward flow through the focus pipes under the normal tide and 1-year storm tide conditions. Before hour 12, the total discharge time series have nearly identical trends under these two conditions. However, the peak of total discharge under the 1-year storm tide condition is about 10% lower than the normal tide condition. Meanwhile, from Figure 9 (b), the maximum inland flood volume for the 1-year storm tide is about 5% higher than the normal tide. The pipeline outlets elevation is higher than the normal tide peak, but lower than the 1-year storm tide peak. Therefore, the 1-year storm tide has a blockage effect on the drainage system and would slow down the draining of inland stormwater.

When the recurrence intervals of storm tide are equal to or higher than 10 years, backward flow would occur at the beginning period of the storms. This means these storm tide events are able to reach to the pipelines in the inland region. Under the 10-year tide condition, the total volume of backward flow

through the focus pipes is $37{,}000m^3$. This volume would occupy a large portion of the storage space of pipeline system and slow down the draining of runoff from the inland region. The blockage effect results in the peak of total discharge under the 10-year tide condition decreased by 22% compared to the normal tide condition, and the maximum inland flood volume increased by 34%.

The total volumes of backward flow are $310{,}000m^3$ and $210{,}000m^3$ under the 50 and 100-year storm tide conditions, respectively. In the current paper, designed storm tides are selected based on the peak water levels; for example, the 100-year tide is 0.04m higher than the 50-year tide. However, the duration of the 50-year tide is about 5 hours longer than the 100-year tide, which is the reason that the 50-year tide caused greater volume of backward flow. The water head near the peaks of 50 and 100-year storm tide events are higher than several flood-prone areas in the inland region. Thus, in the simulation, a portion of the backward flow would exit the pipeline system and cause inundation in these areas. From Figure 9 (b), the maximum flood volumes under the 50 and 100-year tide conditions have more than 70% increase compared to the normal tide condition. Therefore, the surcharge flow on top of the blockage effect on pipeline system greatly exacerbate the flooding in inland region.

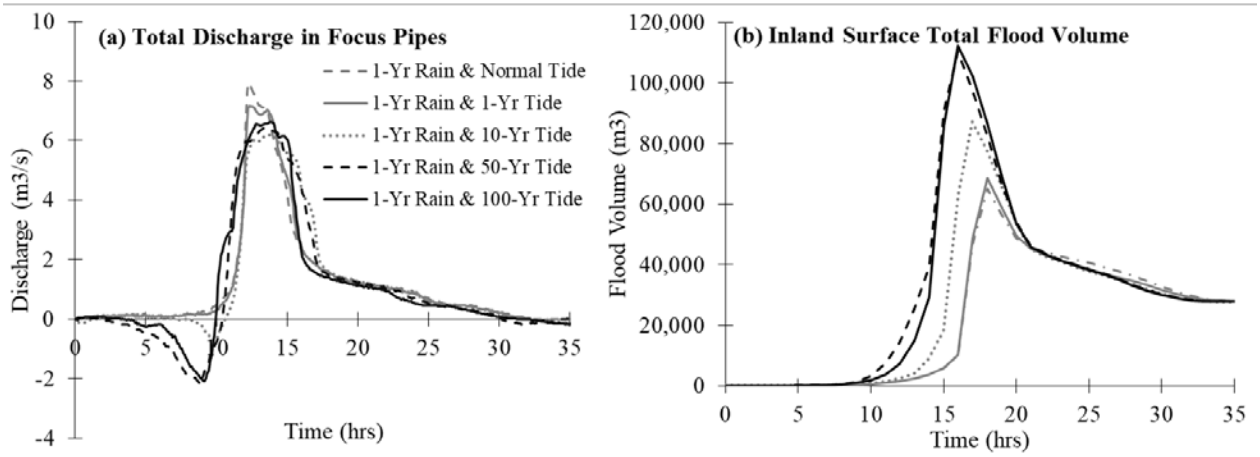

Figure 9. Influence of tide level on the efficiency of the underground pipeline system: (a) total flood volume of inland area under the condition of different storm tide scenarios; (b) total discharge in focus pipes.

3.5 Coastal Floodplain Mapping

The coastal floodplain mapping method is demonstrated by three simulations generated from the 50-year rainfall and 50-year storm tide. In Simulation I, the 50-year tide is the only input, i.e., no rainfall. Simulation II consists of 50-year rain and normal tide. Simulation III consists of 50-year rainfall and 50-year tide. For the focused transect in Figure 1, the maximum water level simulations for these three simulations, along with the land surface elevation profile, are presented in Figure 10. In the tidal zone, the maximum water levels from Simulations I and III have a difference less than 0.01m, which means the impact from rainfall is negligible. In the hydrological zone, the difference between maximum water level simulations from Simulations II and III is less than 0.01m. This indicates that storm tide has minor impact in the hydrological zone, and rainfall is the dominating factor. The transition zone is normally located between the tidal zone and hydrological zone. In transition zone, the maximum water level from Simulation III is higher than both Simulations I and II.

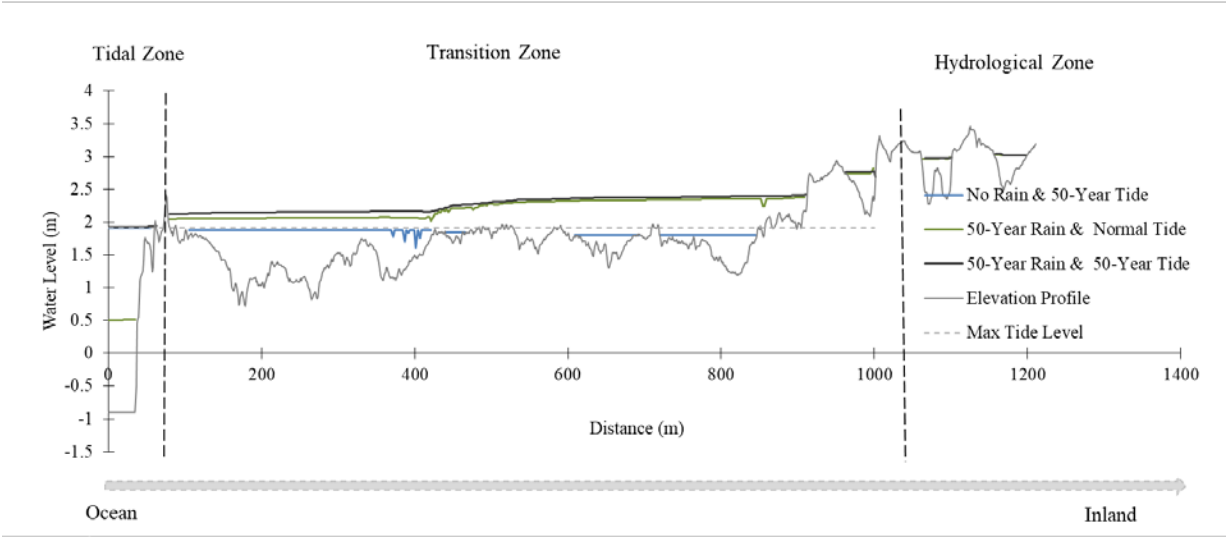

Fig. 10. Land surface elevation profile and simulated maximum water levels across the selected transect for three storm scenarios.

For Simulation III, the spatial extent of different flood zones are identified, as shown in Figure 11. The total inundation area is $1.17 km^2$, which is about 32.5% of the land area. The inundation area includes 7% of the tidal zone, 43% of the hydrological zone, and 50% of the transition zone. The tidal zone is located in a narrow region near the shoreline. The hydrological zone is primarily distributed in inland region. The

transition zone, as originally proposed by Bilskie and Hagen (2018), is located relatively close to the shoreline. However, in this study and in contrast to the Bilskie and Hagen (2018) study, due to the existing of pipeline system, the transition zone can reach to much further inland areas. This is because the strong interaction between rainfall-driven and tidal flooding exists for both the ground surface and underground drainage systems.

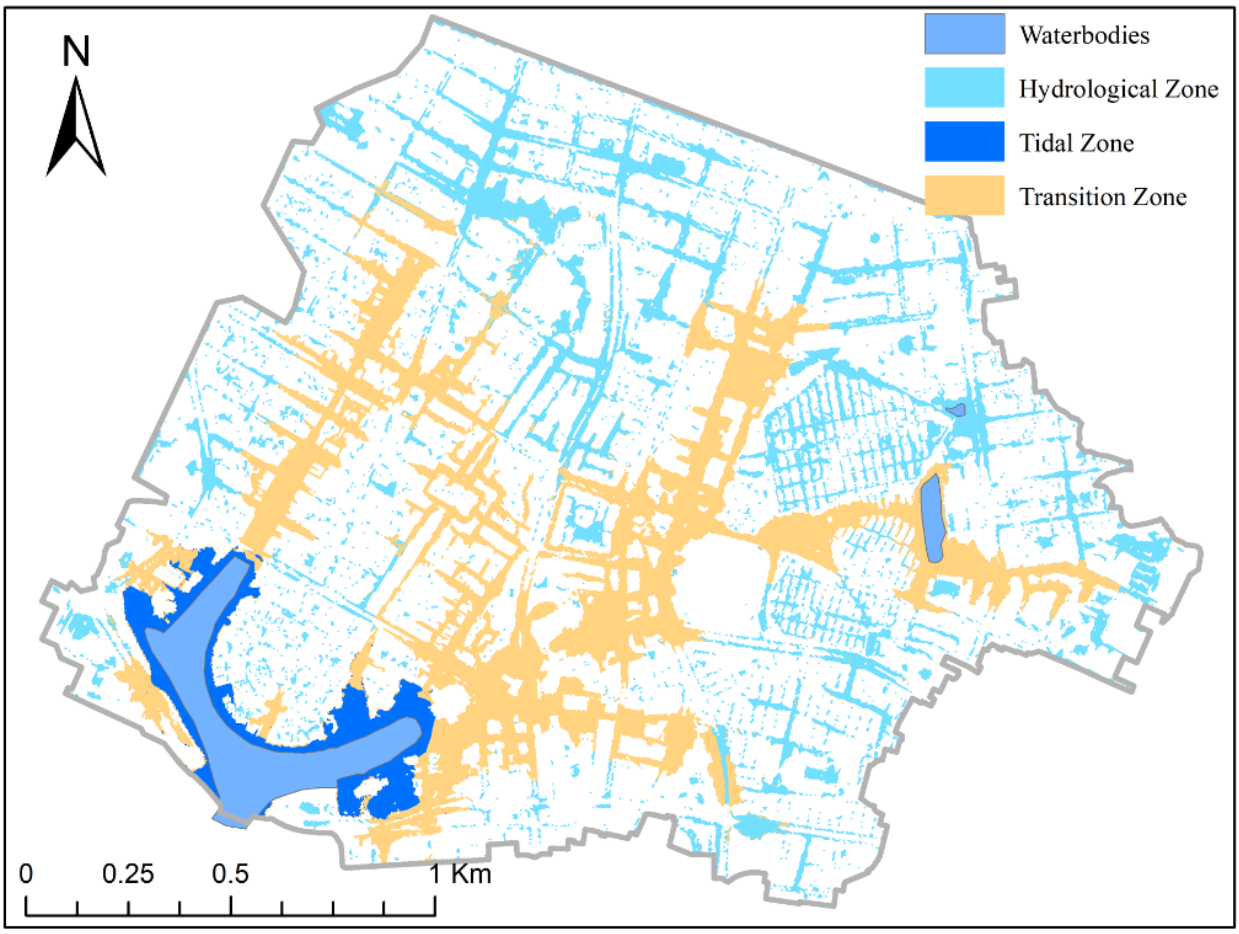

Fig. 11. Flooding zones identified for storm scenario consists of 50-year storm tide and 50-year heavy rainfall

Based on the simulations from the 16 compound storm scenarios in this study, the transition zone index (TZI) was computed and presented in Figure 12. Generally, high TZI locates flood-prone areas where strong interaction exists between storm tide and heavy rainfall. These regions are prone to rainfall-driven flooding due to the relatively low elevation comparing to surround areas. Meanwhile, storm tide would slow down the draining of stormwater from these regions, and in extreme conditions, pipe flow can

become surcharge flow and exacerbate flooding severity. The high TZI areas are normally located in the middle region between shoreline and inland area. The inland region has zero or relatively small TZI, which means rainfall is the dominating factor of flooding. Thus, in the inland region, stormwater control measures (e.g., detention pond or rain garden) are effective flood mitigation strategies. In the near-shoreline region, storm tide is the primary driving factor of flooding because of the small TZI. Therefore, tide control measures (e.g., tide gates or flood walls) can be effective to reduce flood risk. For the high TZI areas, both stormwater and tide control measures can potentially help to reduce the flood risk, and the efficiency and mechanisms can be evaluated and explored using the 1D pipe/2D overland flood model.

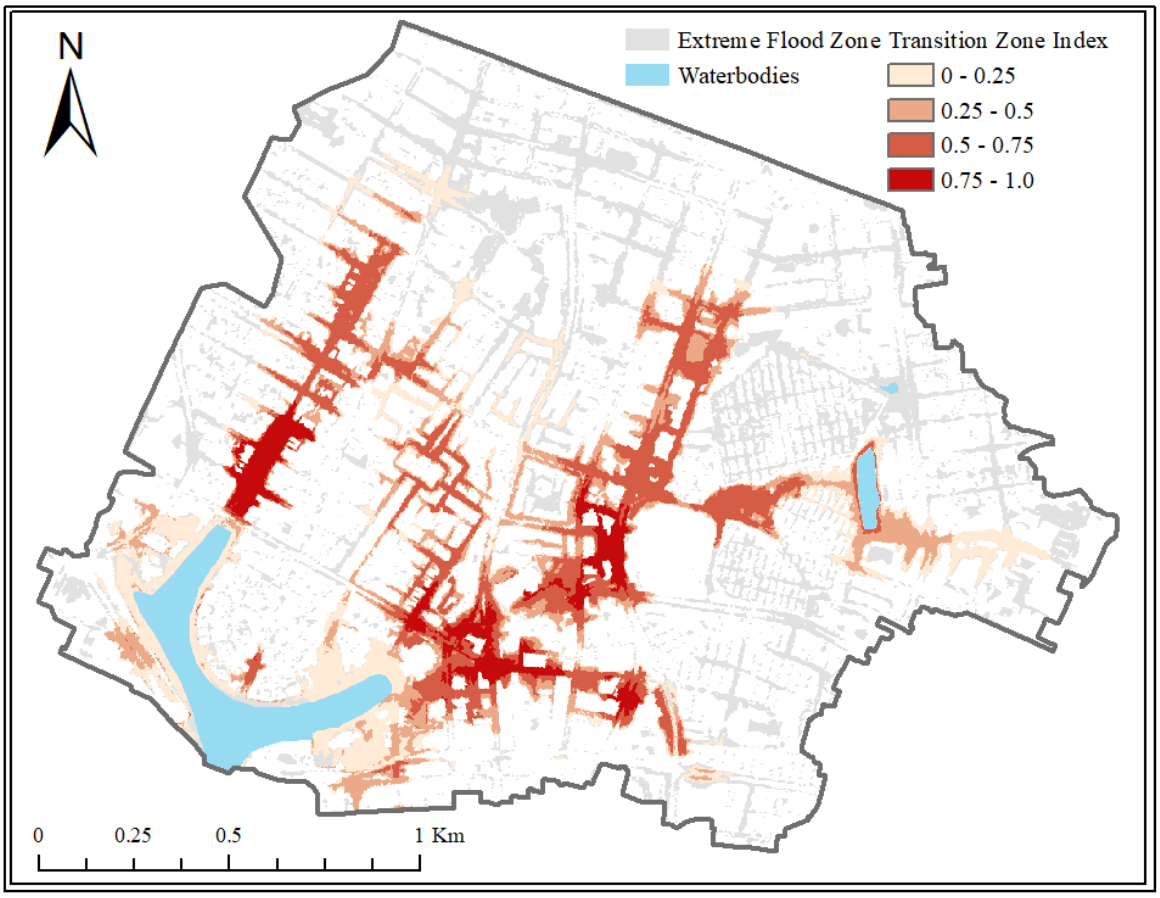

Fig. 12. Transition zone index estimated based on all compound storm scenario simulations

3.6 Flood Mitigation Strategies

In order to demonstrate how the model can be used to aid decision makers when decided between strategies for improving flood resilience within a system, two mitigation strategies were explored for the

case study watershed. In both cases, the TZI maps help decisions makers to anticipate regions within the watershed that will be improved based on the mitigation strategy selected. The first strategy is to install flap gates at certain locations within the drainage system to block backflow from high tide. This strategy is aimed at improving flood resilience for areas in the tidal zone with a low TZI value. The second strategy is to increase the useable capacity of a detention pond within the watershed to increase its capability for flood control. This strategy is targeted areas in the Hydrological Zone with low TZI value could be impacted by either of these two mitigation strategies in complex ways. The ponding depth reduction ratio is defined as the criteria for quantifying the improved resilience of the flood mitigation methods. The ponding depth reduction ratio is defined as

$$Ponding\ Depth\ Reduction\ Ratio = \frac{MPD_{Modified} - MPD_{Original}}{MPD_{Original}} \times 100\% \quad (3)$$

Where, the $MPD_{Modified}$ is the maximum ponding depth simulation from the urban flood model including flood mitigation method, and the $MPD_{Original}$ is the maximum ponding depth simulation from the original version of the urban flood model with no flood reduction measure.

Two methods of using flap gates are discussed in this section. The first method (Version I) is to install flap gates at the 17 outfalls of the drainage system. However, during extreme high tide, overland tidal flooding can reach to near-shoreline region to inundate several pits and manholes, and sea water would enter into the drainage system through these pits and manholes. The region inundated by overland tidal flooding is defined as the tidal floodplain. To further reduce the volume of backward flow from tide, the second method (Version II) is to install flap gates at all pipes covered by the 100-year tidal floodplain. The Version I and II methods were tested on storm scenarios with 1-year rainfall combined with 10 or 100-year storm tide events. The maximum ponding depths were simulated from the urban flood models with and without flap gates. The ponding depth reduction ratio were calculated as shown in Figure 13.

Overall, the reduction of maximum ponding depth can be observed from the simulation in several flood-prone regions after flap gates are installed, also flap gates have greater influence for a more extreme

storm tide event. Under the combined impact of the 1-year rainfall and 10-year tide event, the Version I method is able to reduce the ponding depth by 2% to 5% for several flood-prone areas, and 5% to 15% in a small portion of these flood-prone area. Under the same event, the Version II method generates large area with a reduction ratio between 5 to 15%. For the storm scenarios with 100-year tide, the ponding depth reduction appear more expansive compared with the 10-year tide. However, the reduction ratio from the Version I method is limited to the range of 2 to 15%, and the majority of that is between 2 to 5%. For the Version II method, the maximum ponding depth shows a significant reduction in the upstream flood-prone area. In this case, a large area experiences a ponding depth reduction ratio between 5 to 30%, and several areas have a reduction ratio greater than 30%.

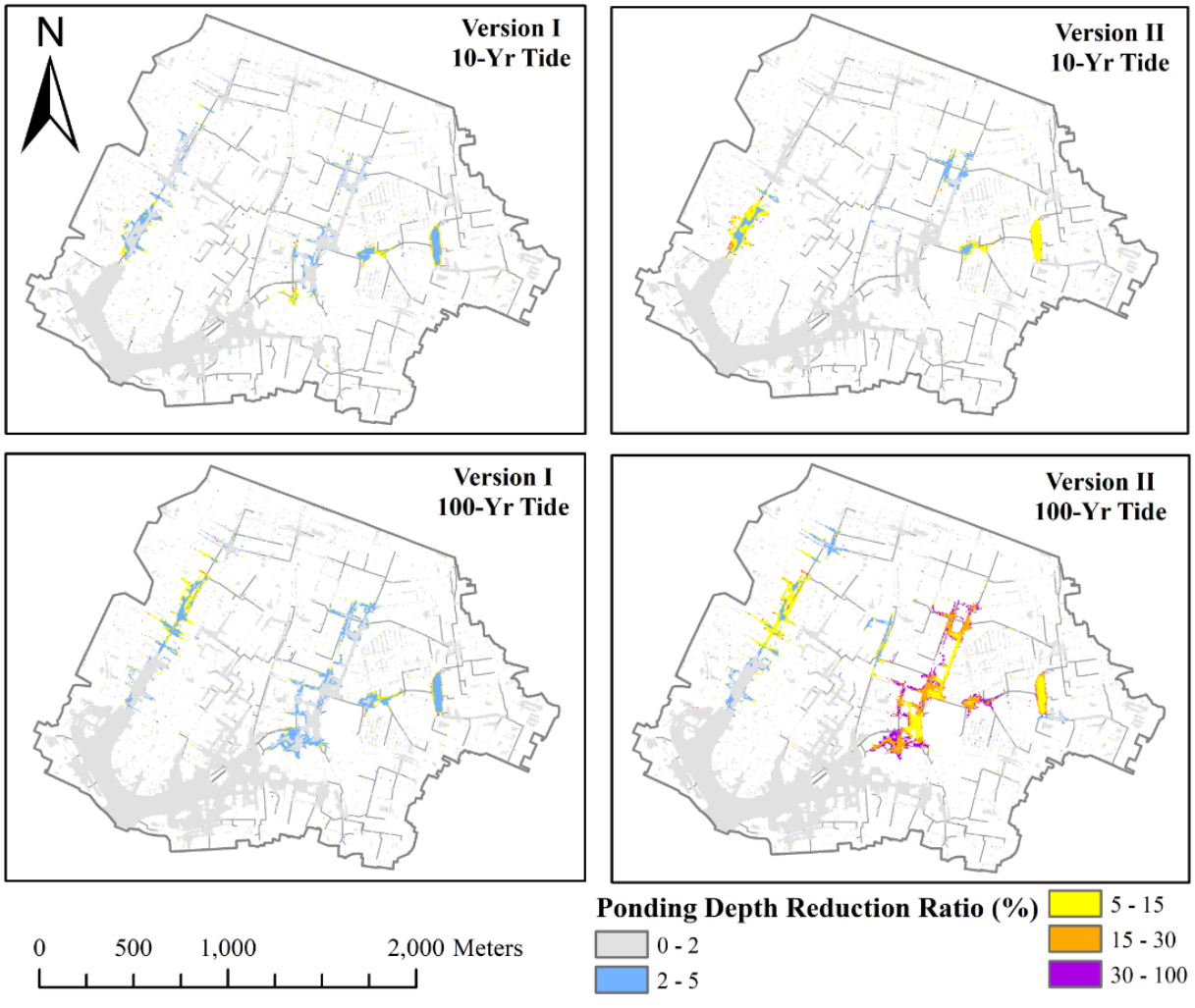

Fig. 13. Ponding depth reduction ratio between simulations with and without flap gates: (Version I) flap gates installed at drainage system outfalls; (Version II) flap gates installed in pipes inside the 100-year tidal floodplain. (Tested storm scenarios: 1-year rainfall with 10 and 100-year storm tide events).

The detention pond in the study domain is a permanent pool of standing water that provides long-term water quality enhancement of stormwater runoff. Stormwater can also be temporarily stored in the detention pond for downstream flood control. The detention pond has a total capacity of about 24,000m^3 and a bed elevation of -1.83m (NAVD88). The detention pond has a normal water level of about 0.35m (NAVD88) and detention storage of about 15,600m^3. The flood control ability of the detention pond is determined by its usable capacity at the beginning of storm events. To enlarge the usable capacity, stormwater control structures can be installed to lower the water level in advance of a forecasted storm. For example, if the water level is lowered to -1m (NAVD88), the detention pond would gain 7,000m^3 extra usable capacity for flood control.

Two initial water level (IWL) scenarios were tested in this section. For the first scenario (IWL I), the IWL was lowered to -1m above NAVD88. The second scenario (IWL II) had an IWL of -1.83m, the bed elevation, meaning the detention pond is dry under the IWL II condition. The IWL II is tested and discussed to represent a best-case scenario for flood risk reduction. The storm scenarios with the joint occurrences of 1 and 10-year rainfall with 1-year tide are selected to analyze the efficiency of flood mitigation when the detention pond is in IWL I and II conditions.

The ponding depth reduction ratios between the maximum ponding depth simulations with lowered IWLs and normal water level of the detention pond are calculated and presented in Figure 14. Generally, lowering the detention pond IWL only influences the flooding in local regions near the pond, and the ponding depth reduction ratios on IWL I and II conditions are very similar for both tested storm scenarios. This is because the usable capacities of the detention pond have relatively small difference (about 2,000m^3) between IWL I and II conditions. With a 1-year rainfall event, the detention pond does not reach to its full capacity under both IWL conditions, and the maximum ponding depths in the region downstream the pond decrease by 2 to 15%. For a 10-year rainfall event, the detention pond does exceed

bankfull levels, and the maximum ponding depths in the downstream region near the pond decrease by 5 to 15%, and a portion of this region has more than a 15% ponding depth reduction ratio. A 2 to 15% reduction ratio occurs in the further downstream. The most significant flood mitigation appears on the southeastern portion of the detention pond drainage area due to increased capacity to store rainfall runoff generated from this area.

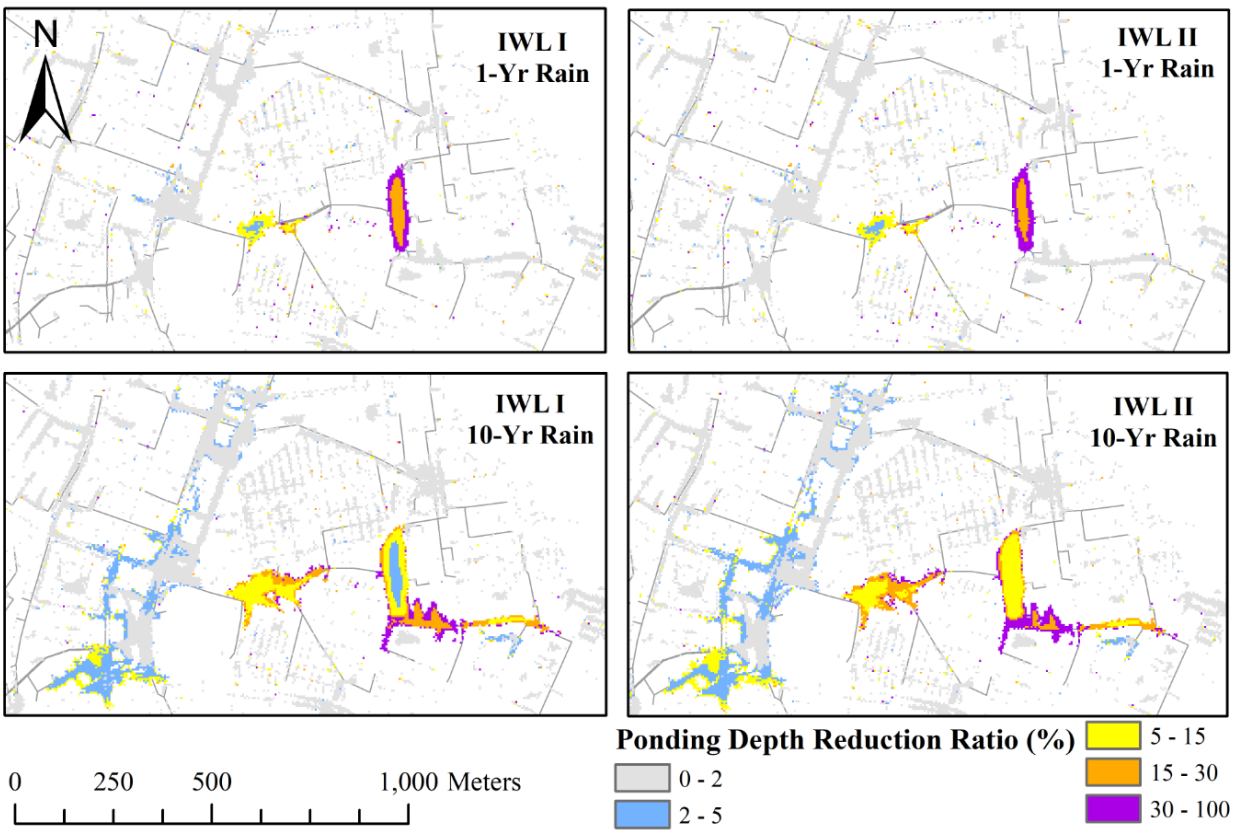

Fig. 14. Ponding depth reduction ratio between the maximum ponding depth simulations on lowered initial water levels and normal water level of the detention pond: (IWL I) initial water level lower to -1m; (IWL II) initial water level lower to -1.84m. (Tested storm scenarios**:** 1 and 10-year rainfall with 1-year tide event).

4. Conclusions

An overarching objective of this study was to develop methodologies to enhance the understanding of flood risk within coastal urban watersheds. To this end, we modeled how overland flooding in an urban watershed with stormwater drainage infrastructure is affected by storm tide and rainfall events with varying return periods. The study area is located in Norfolk, VA, USA, a city prone to recurrent flooding

challenge, was the case study system for the study. The 1 to 100-year storm tide events were designed based on storm tides that happened during historical hurricanes impacting the Virginia coastline. A series of rainfall events with return periods varying from 1 to 100-year were designed based on the NOAA Atlas 14 precipitation frequency estimates (Bonnin et. al., 2006). These design storm tide and rainfall events were combined to a series of compound storm scenarios. A coupled 1D pipe/2D overland hydrodynamic model was built for the study watershed using the TUFLOW model. The model outputs included detailed flooding information on both land surface and underground pipeline system, which allows to assess flood risk and understand the contribution of flooding from individual or combined factors. Floodplain maps and a new transition zone index (TZI) were created to communicate regions of the watershed under risk of flooding due to tide and rainfall-driven mechanisms. The 1D pipe/2D overland flood model and floodplain visualizations are a powerful tool to evaluate the efficiency of different flood mitigation strategies, as a demonstrated for two flood mitigation methods.

Results show how the capacity of stormwater drainage system is highly sensitive to storm tide levels. Based on model simulations, event with a 1-year tide is able to partially submerge the pipeline outlets and has an impact on the pipeline capacity. Storm tide events with return periods greater than or equal to 10 years would significantly reduce the drainage capacity. Extreme storm tide events, for example a 50 and 100-year tide, would cause flooding within the watershed due to the backing-up and day lighting of sea water traveling through stormwater drainage infrastructure. Even for smaller tide events, model simulations show that rainfall driven flooding combined with reduced capacity of the drainage infrastructure caused by tailwater conditions can cause significant flooding in inland regions. Due to the low gradient of the stormwater drainage infrastructure, which is common in many coastal urban areas, this interaction between rainfall-driven flow and sea water flow traveling through the pipe system can influence flooding far into the watershed.

This study provides a methodology that can be repeated for other coastal urban watersheds to better understand the influence of storm tide and rainfall-driven flooding through floodplain maps. The

628 coastal floodplain mapping method proposed in Bilskie and Hagen's study (2018) was applied to the
629 urban watershed in the current study. In Bilskie and Hagen's study (2018), the study area is located in a
630 rural area, and the interaction between rainfall-driving and tidal flooding is primarily within the region
631 close to the shoreline. However, in this study, we extended on past work to include the stormwater
632 drainage system, showing that the transition zone can reach much further inland due to the underground
633 stormwater drainage system. The transition zone index (TZI) was defined to represent the likelihood of a
634 location under the impact of strong interaction between tidal and rainfall-driven flooding. In areas with
635 low TZI, flood risk is primarily caused by individual factors. Therefore, flood mitigation measures
636 targeting to individual flood mechanisms can be effective ways to reduce flood risk in these parts of the
637 watershed. For the high TZI areas, both stormwater and tide control measures can potentially assist to
638 reduce the flood risk, and the efficiency and mechanisms can be evaluated and explored using the 1D
639 pipe/2D overland flood model.

640 Lastly, the flood model and floodplain visualization is a powerful tool to evaluate the efficiency
641 of different flood mitigation strategies. As a demonstration, two flood mitigation methods were tested in
642 this study: one targeting rainfall-driven flooding and the second targeting tidal-driven flooding. The
643 model simulations show how both methods would be able to reduce the flood risk for certain flood-prone
644 regions of the watershed. Because the floodplain map helps to visualize regions of the watershed where
645 tide, rainfall, or a combination of these two mechanisms cause flooding, it is easier to see how mitigation
646 strategies improve flood resilience. This methodology can be of a significant value to cities and
647 communities as they work to improve resilience for a host of services that can be impacted by flood risk.

648 The presented model will be used in a future study to explore several aspects of compound storm
649 tide and rainfall-driven flooding. In this study, only tide level data is considered at the boundary as the
650 tide input while tidal flow velocity may have a significant effect on tidal flooding and the function of
651 drainage system. Future research should focus on coupling a hydrodynamic storm surge model with the
652 inland hydrodynamic model to account for these processes. Furthermore, this study is focused on present

sea level. However, climate change impacts include increases in rainfall intensity and relative sea level rise (RSLR), which could substantially increase the severity of flood risk in the study area. Future assessments using this model will aim to quantify the impacts of changing climatic conditions on flooding risk.

Acknowledgements

This work was supported by the National Science Foundation under the award number 1735587. The authors wish to acknowledge the BMT for the TUFLOW HPC license and kindly help on model building and problem solving. We would also like to acknowledge the University of Virginia Advance Research Computing Services for providing the GPUs computing resource. NT acknowledges support from the Department of Transportation through Mid-Atlantic Transportation Sustainability-University Transportation Center (MATS-UTC).

References

Archetti, R., Bolognesi, A., Casadio, A., Maglionico, M., 2011. Development of flood probability charts for urban drainage network in coastal areas through a simplified joint assessment approach. Hydrol. Earth Syst. Sci. 15, 3115–3122. https://doi.org/10.5194/hess-15-3115-2011.

Batten, B., Rosenberg, S., Sreetharan, M., 2017. Joint Occurrence and Probabilities of Tides and Rainfall. City of Virginia Beach. https://www.vbgov.com/government/departments/public-works/comp-sea-level-rise/Documents/joint-occ-prob-of-tides-rainfall-4-24-18.pdf.

Bilskie, M. V, Hagen, S.C., 2018. Defining flood zone transitions in low-gradient coastal regions. Geophys. Res. Lett. 45, 2761–2770. https://doi.org/https://doi.org/10.1002/2018GL077524.

Bonnin, G.M., Martin, D., Lin, B., Parzybok, T., Yekta, M., Riley, D., 2006. NOAA Atlas 14 Precipitation-Frequency Atlas of the United States. Silver Spring, Maryland. http://www.nws.noaa.gov/oh/hdsc/PF_documents/Atlas14_Volume2.pdf.

Bryndal, T., Franczak, P., Kroczak, R., Cabaj, W., Kołodziej, A., 2017. The impact of extreme rainfall and flash floods on the flood risk management process and geomorphological changes in small Carpathian catchments: a case study of the Kasiniczanka river (Outer Carpathians, Poland). Nat. Hazards 88, 95–120. https://doi.org/10.1007/s11069-017-2858-7

Castrucci, L., Tahvildari, N., 2018. Modeling the Impacts of Sea Level Rise on Storm Surge Inundation in Flood-Prone Urban Areas of Hampton Roads, Virginia. Mar. Technol. Soc. J. 52, 92–105. https://doi.org/10.4031/MTSJ.52.2.11.

Chen, A.S., Evans, B., Djordjević, S., Savić, D.A., 2012. A coarse-grid approach to representing building blockage effects in 2D urban flood modelling. J. Hydrol. 1–16. https://doi.org/10.1016/j.jhydrol.2012.01.007.

Dawson, R.J., Speight, L., Hall, J.W., Djordjevic, S., Savic, D., Leandro, J., 2008. Attribution of flood risk in urban areas. J. Hydroinformatics 10, 275. https://doi.org/10.2166/hydro.2008.054.

FEMA, 2018. Guidance for flood risk analysis and mapping: coastal general study considerations. https://www.fema.gov/media-library/assets/documents/34953.

Fohringer, J., Dransch, D., Kreibich, H., Schröter, K., 2015. Social media as an information source for rapid flood inundation mapping. Nat. Hazards Earth Syst. Sci. 15, 2725–2738. https://doi.org/10.5194/nhess-15-2725-2015.

Garcia, R., Restrepo, P., DeWeese, M., Ziemer, M., Palmer, J., Thornburg, J., Lacasta, A., 2015. Advanced GPU paralellization for two-dimensional operational river flood forecasting, in: In 36th International Association for Hydro-Environment Engineering and Research World Congress. The Hague, Netherlands.

Hallegatte, S., Green, C., Nicholls, R.J., Corfee-Morlot, J., 2013. Future flood losses in major coastal cities. Nat. Clim. Chang. 3, 802–806. https://doi.org/10.1038/nclimate1979.

Hanson, S., Nicholls, R., Ranger, N., Hallegatte, S., Corfee-Morlot, J., Herweijer, C., Chateau, J., 2011. A global ranking of port cities with high exposure to climate extremes. Clim. Change 104, 89–111. https://doi.org/10.1007/s10584-010-9977-4.

Hunter, N.M., Bates, P.D., Neelz, S., Pender, G., Villanueva, I., Wright, N.G., Liang, D., Falconer, R.A., Lin, B., Waller, S., Crossley, A.J., Mason, D.C., 2008. Benchmarking 2D hydraulic models for urban flooding. Proc. Inst. Civ. Eng. - Water Manag. 161, 13–30. https://doi.org/10.1680/wama.2008.161.1.13.

Huxley, C., Syme, B., 2016. TUFLOW GPU-best practice advice for hydrologic and hydraulic model simulations. in: Proceedings of the 37th Hydrology and Water Resources Symposium (HWRS). Queenstown, New Zealand.

Karamouz, M., Razmi, A., Nazif, S., Zahmatkesh, Z., 2017. Integration of inland and coastal storms for flood hazard assessment using a distributed hydrologic model. Environ. Earth Sci. 76, 1–17. https://doi.org/10.1007/s12665-017-6722-6

717 Karamouz, M., F., Zahmatkesh, Z., Goharian, E., S.M., Nazif, S., 2015. Combined Impact of
718 Inland and Coastal Floods : Mapping Knowledge Base for Development of Planning
719 Strategies 141, 1–16. https://doi.org/10.1061/(ASCE)WR.1943-5452.0000497.

720 Li, H., Lin, L., Burks-Copes, K.A., 2013. Modeling of coastal inundation, storm surge, and
721 relative sea-level rise at Naval Station Norfolk, Norfolk, Virginia, U.S.A. J. Coast. Res. 29,
722 18–30. https://doi.org/10.2112/JCOASTRES-D-12-00056.1.

723 Lian, J.J., Xu, K., Ma, C., 2013. Joint impact of rainfall and tidal level on flood risk in a coastal
724 city with a complex river network: A case study of Fuzhou City, China. Hydrol. Earth Syst.
725 Sci. 17, 679–689. https://doi.org/10.5194/hess-17-679-2013.

726 Loftis, J.D., Wang, H., Forrest, D., Rhee, S., Nguyen, C., 2017. Emerging flood model validation
727 frameworks for street-level inundation modeling with StormSense, in: Proceedings of the
728 2nd International Workshop on Science of Smart City Operations and Platforms
729 Engineering. Pittsburgh, PA, pp. 13–18. https://doi.org/10.1145/3063386.3063764.

730 Mark, O., Weesakul, S., Apirumanekul, C., Aroonnet, S. B., and Djordjević, S., 2004. Potential
731 and limitations of 1D modeling of urban flooding. J. Hydrol. (Amsterdam), 299(3–4), 284–
732 299.

733 McCuen, R.H., 1998. Hydrologic Analysis and Design, Second. ed, Prentice Hall. New Jersey.
734 ISBN: 9786468600.

735 Merkel, W.H., Moody, H.F., Quan, Q.D., 2015. Design rainfall distributions based on NOAA
736 Atlas 14 rainfall depths and durations. Beltsville, MD.
737 https://www.wcc.nrcs.usda.gov/ftpref/wntsc/H&H/rainDist/FIHMC_2015_Rainfall_Distrib
738 ution_NOAA_14_Merkel.pdf.

739 Middleton, S.E., Middleton, L., Modafferi, S., 2014. Real-time crisis mapping of natural
740 disasters using social media. Soc. Intell. Technol. 29, 9–17.
741 https://doi.org/10.1109/MIS.2013.126.

742 Morsy, M.M., Goodall, J.L., O'Neil, G.L., Sadler, J.M., Voce, D., Hassan, G., Huxley, C., 2018.
743 A cloud-based flood warning system for forecasting impacts to transportation infrastructure
744 systems. Environ. Model. Softw. 107, 231–244.
745 https://doi.org/10.1016/j.envsoft.2018.05.007.

746 NWS, 2016. The hurricane history of central and eastern Virginia.
747 https://www.weather.gov/media/akq/miscNEWS/hurricanehistory.pdf

748 Ray, T., Stepinski, E., Sebastian, A., Bedient, P.B., 2011. Dynamic modeling of storm surge and
749 inland flooding in a Texas coastal floodplain. J. Hydraul. Eng. 137, 1103–1110.
750 https://doi.org/10.1061/(ASCE)HY.1943-7900.0000398.

751 Sadler, J.M., Goodall, J.L., Morsy, M.M., Spencer, K., 2018. Modeling urban coastal flood
752 severity from crowd-sourced flood reports using Poisson regression and Random Forest. J.
753 Hydrol. 559, 43–55. https://doi.org/10.1016/j.jhydrol.2018.01.044.

754 Sadler, J.M., Haselden, N., Mellon, K., Hackel, A., Son, V., Mayfield, J., Blase, A., Goodall,
755 J.L., 2017. Impact of sea-level rise on roadway flooding in the Hampton Roads Region,
756 Virginia. J. Infrastruct. Syst. 23, 05017006. https://doi.org/10.1061/(ASCE)IS.1943-
757 555X.0000397.

758 Silva-Araya, W.F., Santiago-Collazo, F.L., Gonzalez-Lopez, J., Javier Maldonado-Maldonado,
759 2018. Dynamic modeling of surface runoff and storm surge during hurricane and tropical
760 storm events. Hydrology 5, 1–28. https://doi.org/10.3390/hydrology5010013.

761 Smith, R.A.E., Bates, P.D., Hayes, C., 2012. Evaluation of a coastal flood inundation model
762 using hard and soft data. Environ. Model. Softw. 30, 35–46.
763 https://doi.org/10.1016/j.envsoft.2011.11.008.

764 Svensson, C., Jones, D.A., 2004. Dependence between sea surge, river flow and precipitation in
765 south and west Britain. Hydrol. Earth Syst. Sci. 8, 973–992. https://doi.org/10.5194/hess-8-
766 973-2004.

767 Syme, W.J., 2008. Flooding in Urban Areas-2D Modelling Approaches for Buildings and
768 Fences, in: 9th National Conference on Hydraulics in Water Engineering. Darwin City,
769 Australia, pp. 23–26.

770 Syme, W.J., 2001. TUFLOW–Two & one-dimensional Unsteady FLOW Software for Rivers,
771 Estuaries and Coastal Waters, in: Paper Presented at the IEAust Water Panel Seminar and
772 Workshop on 2d Flood Modelling. Sydney,Australia, pp. 2–9.

773 Upadhyaya, J.K., Biswas, N., Tam, E., 2014. A review of infrastructure challenges: assessing
774 stormwater system sustainability. Can. J. Civ. Eng. 41, 483–492.
775 https://doi.org/10.1139/cjce-2013-0430.

776 Wahl, T., Jain, S., Bender, J., Meyers, S.D., Luther, M.E., 2015. Increasing risk of compound
777 flooding from storm surge and rainfall for major US cities. Nat. Clim. Chang. 5, 1093–
778 1097. https://doi.org/10.1038/nclimate2736.

779 Wang, Y., Colby, J. D., Mulcahy, K. A., 2002. An efficient method for mapping flood extent in a
780 coastal floodplain using Landsat TM and DEM data. International Journal of Remote
781 Sensing. 23 (18), 3681-3696. https://doi.org/10.1080/01431160110114484

782 Woodruff, J.D., Irish, J.L., Camargo, S.J., 2013. Coastal flooding by tropical cyclones and sea-
783 level rise. Nature 504, 44–52. https://doi.org/10.1038/nature12855.

784 Xu, K., Ma, C., Lian, J., Bin, L., 2014. Joint probability analysis of extreme precipitation and
785 storm tide in a coastal city under changing environment. PLoS One 9.
786 https://doi.org/10.1371/journal.pone.0109341.

787 Yazdanfar, Z., Sharma, A., 2015. Urban drainage system planning and design - Challenges with
788 climate change and urbanization: A review. Water Sci. Technol. 72, 165–179.
789 https://doi.org/10.2166/wst.2015.207.

790 Zheng, F., Westra, S., Sisson, S.A., 2013. Quantifying the dependence between extreme rainfall
791 and storm surge in the coastal zone. J. Hydrol. 505, 172–187.
792 https://doi.org/10.1016/j.jhydrol.2013.09.054.

793

794

795

796

797 **Appendix A**

798 The watershed is urbanized and flow has complex patterns and paths through building areas.
799 These buildings dissipate energy by forcing the flow to change its direction and speed. In prior studies,
800 the buildings in the 2D model domain have been represented by increasing the roughness coefficient,
801 blocking out of buildings, applying energy loss coefficient in building areas, and setting the buildings as
802 porous elements (Hunter et. al., 2008; Syme, 2008; Chen et. al., 2012). In this study, one assumption is
803 that no water would enter into buildings during simulations. Therefore, the method of blocking out of
804 buildings is the only satisfactory option based on this assumption. As shown in Figure A1, the areas
805 inside building outlines are deactivated from the 2D domain. To make sure no stormwater from rainfall
806 lost by deactivating the buildings areas, a building representation method is proposed in this study,
807 including three major steps: I) deactivate areas inside building outlines from the 2D domain; II) build
808 polygons that includes groups of buildings; and III) apply the rainfall falling on the building areas to the
809 buffered polygon around each group of buildings. The building roofs are designed to drain rain water
810 rapidly and completely. The assumption behind the building representation method is that rain water can
811 drain out of building roofs without any loss of rain water and no delay time from transferring the water

from precipitation to ground. This method is reasonable for the study domain where most of its buildings are residential houses with relatively small roof areas.

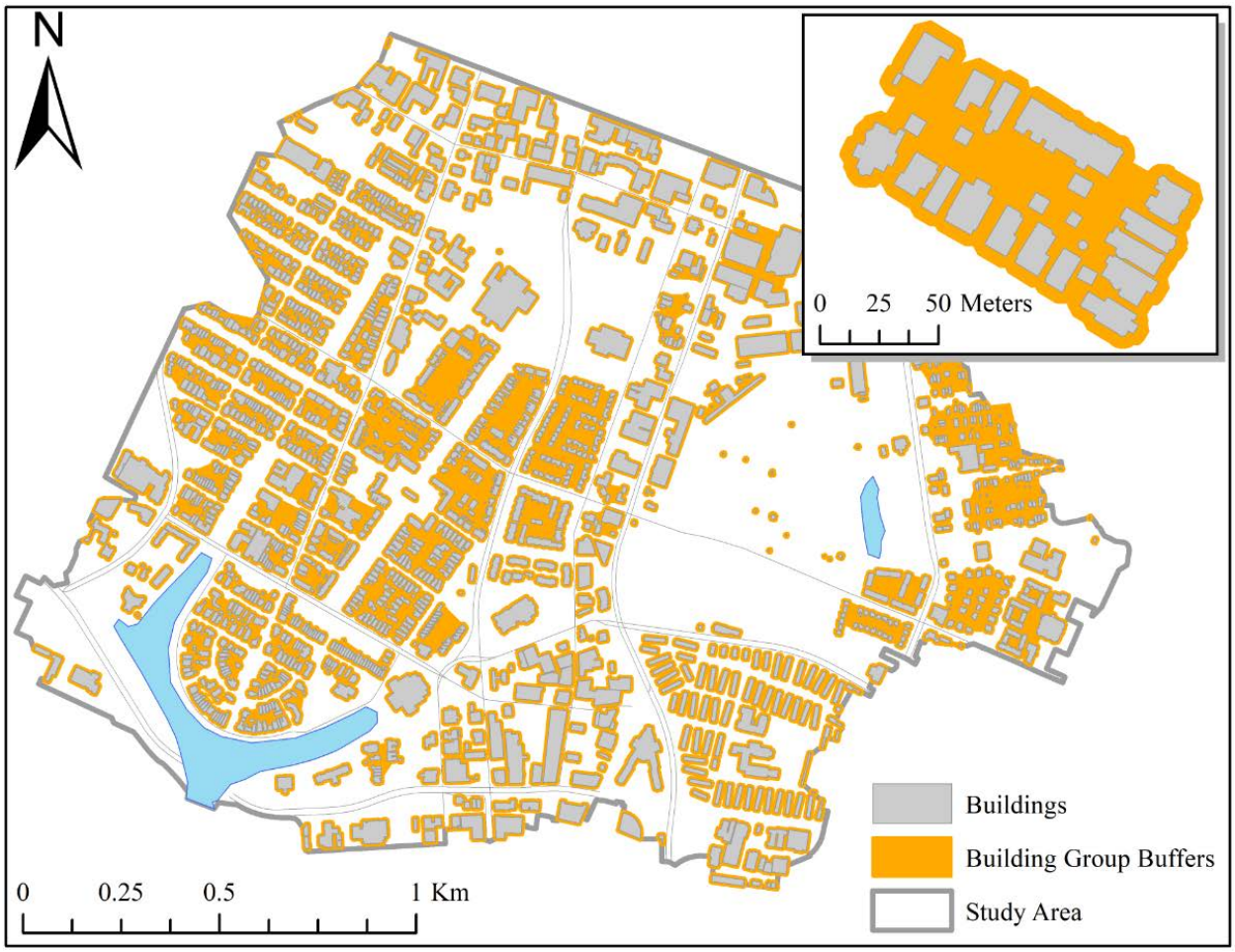

Fig. A1. Representation of buildings in the urban flood model.